Tenth-order electron anomalous magnetic moment: Contribution of diagrams without closed lepton loops

Tatsumi Aoyama, Masashi Hayakawa, Toichiro Kinoshita, and Makiko Nio

Phys. Rev. D **91**, 033006 — Published 24 February 2015

DOI: 10.1103/PhysRevD.91.033006

Tenth-Order Electron Anomalous Magnetic Moment — Contribution of Diagrams without Closed Lepton Loops

Tatsumi Aoyama,[1,5] Masashi Hayakawa,[2,5] Toichiro Kinoshita,[3,4,5] and Makiko Nio[5]

[1]*Kobayashi-Maskawa Institute for the Origin of Particles and the Universe (KMI), Nagoya University, Nagoya, 464-8602, Japan*

[2]*Department of Physics, Nagoya University, Nagoya, 464-8602, Japan*

[3]*Laboratory for Elementary Particle Physics, Cornell University, Ithaca, NY, 14853, U.S.A.*

[4]*Amherst Center for Fundamental Interactions, Department of Physics, University of Massachusetts, Amherst, MA, 01003, U.S.A.*

[5]*Nishina Center, RIKEN, Wako, 351-0198, Japan*

Abstract

This paper presents a detailed account of evaluation of the electron anomalous magnetic moment a_e which arises from the gauge-invariant set, called Set V, consisting of 6354 tenth-order Feynman diagrams without closed lepton loops. The latest value of the sum of Set V diagrams evaluated by the Monte-Carlo integration routine VEGAS is 8.726 $(336)(\alpha/\pi)^5$, which replaces the very preliminary value reported in 2012. Combining it with other 6318 tenth-order diagrams published previously we obtain 7.795 $(336)(\alpha/\pi)^5$ as the complete mass-independent tenth-order term. Together with the improved value of the eighth-order term this leads to $a_e(\text{theory}) = 1\,159\,652\,181.643\,(25)(23)(16)(763)\times10^{-12}$, where first three uncertainties are from the eighth-order term, tenth-order term, and hadronic and elecroweak terms. The fourth and largest uncertainty is from $\alpha^{-1} = 137.035\,999\,049\,(90)$, the fine-structure constant derived from the rubidium recoil measurement. $a_e(\text{experiment}) - a_e(\text{theory}) = -0.91\,(0.82)\times10^{-12}$. Assuming the validity of the standard model, we obtain the fine-structure constant $\alpha^{-1}(a_e) = 137.035\,999\,1570\,(29)(27)(18)(331)$, where uncertainties are from the eighth-order term, tenth-order term, hadronic and electroweak terms, and the measurement of a_e. This is the most precise value of α available at present and provides a stringent constraint on possible theories beyond the standard model.

PACS numbers:

I. INTRODUCTION AND SUMMARY

The anomalous magnetic moment of the electron, $a_e \equiv (g-2)/2$, has played an important role in testing the validity of quantum electrodynamics (QED) and the standard model of particle physics. The latest measurement of a_e by the Harvard group has reached the precision of 0.24×10^{-9} [1, 2]:

$$a_e(\mathrm{HV08}) = 1\ 159\ 652\ 180.73\ (0.28) \times 10^{-12} \quad [0.24\mathrm{ppb}]\ . \tag{1}$$

A new apparatus for measuring $g-2$ of electron and positron with even higher precision is being constructed by the same group [3]. In order to test QED to such a precision it is necessary to have a theoretical value of the tenth-order term since

$$(\alpha/\pi)^5 \sim 0.07 \times 10^{-12}, \tag{2}$$

where α is the fine-structure constant.

In the standard model the contribution to a_e comes from three types of interactions, electromagnetic, hadronic, and electroweak, which may be written as

$$a_e = a_e(\mathrm{QED}) + a_e(\mathrm{hadronic}) + a_e(\mathrm{electroweak}), \tag{3}$$

although a_e(hadronic) contains contribution of electromagnetic interaction and a_e(electroweak) contains contribution of electromagnetic and hadronic interactions in higher orders. In the framework of the standard model the dominant contribution comes from a_e(QED). a_e(hadronic) and a_e(electroweak) provide only small corrections. However the latter two cannot be ignored in comparing theory with measurements.

The QED contribution can be evaluated by the perturbative expansion in α/π:

$$a_e(\mathrm{QED}) = \sum_{n=1}^{\infty} \left(\frac{\alpha}{\pi}\right)^n a_e^{(2n)}, \tag{4}$$

where $a_e^{(2n)}$ is finite due to the renormalizability of QED and may be written in general as

$$a_e^{(2n)} = A_1^{(2n)} + A_2^{(2n)}(m_e/m_\mu) + A_2^{(2n)}(m_e/m_\tau) + A_3^{(2n)}(m_e/m_\mu, m_e/m_\tau) \tag{5}$$

to exhibit the dependence on the muon mass and tau-particle mass. We use the electron-muon mass ratio $m_e/m_\mu = 4.836\ 331\ 66\ (12) \times 10^{-3}$ and the electron-tau mass ratio $m_e/m_\tau = 2.875\ 92\ (26) \times 10^{-4}$ [4].

The first three terms of $A_1^{(2n)}$ are known analytically [5–8]. Their numerical values are

$$\begin{aligned} A_1^{(2)} &= 0.5, \\ A_1^{(4)} &= -0.328\ 478\ 965\ 579\ 193\ldots, \\ A_1^{(6)} &= 1.181\ 241\ 456\ldots. \end{aligned} \tag{6}$$

The value of $A_1^{(8)}$, which has contributions from 891 Feynman diagrams, is obtained mostly by numerical integration [9]. It is being improved continually by further numerical work. The latest value

$$A_1^{(8)} = -1.912\ 98\ (84), \tag{7}$$

obtained by a substantial increase in the sampling statistics of VEGAS [10] calculation, is a factor 2.4 improvement over the published result [9].

The term $A_1^{(10)}$ has contributions from 12,672 vertex diagrams, which may be classified into six gauge-invariant sets, further subdivided into 32 gauge-invariant subsets depending on the type of lepton loop subdiagrams. Thus far, the results of numerical evaluation of 31 gauge-invariant subsets, which consists of 6318 vertex diagrams, have been published [11–20]. The results of all 10 subsets of Set I, consisting of 208 vertex diagrams, have been confirmed by Ref. [21]. All these diagrams have closed lepton loops and thus contribute also to $A_2^{(10)}$ and/or $A_3^{(10)}$.

The remaining set, called Set V, consists of 6354 Feynman diagrams which do not have closed lepton loop (denoted as q-type diagrams). It is the largest and most difficult one to evaluate. This paper presents a detailed account of evaluation of Set V diagrams, and gives the latest numerical value. The presented value is more accurate and reliable than the preliminary one reported in Ref. [9], not only because of the increase of the statistics of Monte-Carlo integration, but also by the incorporation of the qualitative improvements explained in Section IV.

Integrals of the Set V are huge and complicated so that their evaluation requires an enormous amount of work. A systematic and fully automatic approach is an absolute necessity to carry out such a project. To meet this challenge we have developed an algorithm GENCODEN [22, 23] which converts automatically the diagrammatic information, specifying how virtual photon lines are attached to the lepton lines, into a FORTRAN code free from ultraviolet and infrared divergences.

The evaluation of the 10th-order diagrams boils down to the numerical integration on a 13-dimensional unit cube onto which a hyperplane of 14 Feynman parameters is mapped. The integrals are evaluated by the adaptive-iterative Monte-Carlo integration routine VEGAS [10]. For this calculation, the RIKEN Supercomputing Systems RSCC and RICC are used intensively. The results are summarized in Table I. Auxiliary quantities required for restoring the standard on-shell renormalization are listed in Table II. From these Tables we obtain

$$A_1^{(10)}[\text{Set V}] = 8.726\ (336). \tag{8}$$

Adding this to the values of the other 31 gauge-invariant sets, which were evaluated and published previously [11–20], we now have an improved value of the sum of all 12,672 diagrams of tenth-order

$$A_1^{(10)} = 7.795\ (336), \tag{9}$$

which replaces the very preliminary value reported in Ref. [9].

The mass-dependent terms A_2 and A_3 of the fourth and sixth orders are known [24–29],

$$\begin{aligned}
A_2^{(4)}(m_e/m_\mu) &= 5.197\ 386\ 67\ (26) \times 10^{-7}, \\
A_2^{(4)}(m_e/m_\tau) &= 1.837\ 98\ (34) \times 10^{-9}, \\
A_2^{(6)}(m_e/m_\mu) &= -7.373\ 941\ 55\ (27) \times 10^{-6}, \\
A_2^{(6)}(m_e/m_\tau) &= -6.583\ 0\ (11) \times 10^{-8}, \\
A_3^{(6)}(m_e/m_\mu, m_e/m_\tau) &= 1.909\ (1) \times 10^{-13},
\end{aligned} \tag{10}$$

and those of eighth and tenth order terms can be found in Refs. [11–20, 30]

$$\begin{aligned}
A_2^{(8)}(m_e/m_\mu) &= 9.161\ 970\ 703\ (373) \times 10^{-4}, \\
A_2^{(8)}(m_e/m_\tau) &= 7.429\ 24\ (118) \times 10^{-6}, \\
A_3^{(8)}(m_e/m_\mu, m_e/m_\tau) &= 7.4687\ (28) \times 10^{-7}, \\
A_2^{(10)}(m_e/m_\mu) &= -0.003\ 82\ (39).
\end{aligned} \tag{11}$$

Our evaluation of $A_2^{(8)}(m_e/m_\mu)$ and $A_2^{(8)}(m_e/m_\tau)$ has been confirmed by the analytic calculations of Refs. [30, 31].

Recently, the possible non-perturbative effect of QED to the order of α^5 of the electron $g-2$ was pointed out [32, 34], but shown to be absent [33–35] in accord with the earlier

studies of Refs. [36, 37] applied to the electron $g-2$. Ref. [38] presents an approach different from those of Refs. [33–35].

The latest values of the leading order and next-to-leading order (NLO) contributions of the hadronic vacuum-polarization (v.p.) are given in Ref. [39]

$$\begin{aligned} a_e(\text{had. v.p}) &= 1.866\ (10)_{\text{exp}}\ (5)_{\text{rad}} \times 10^{-12}, \\ a_e(\text{NLO had. v.p}) &= -0.2234\ (12)_{\text{exp}}\ (7)_{\text{rad}} \times 10^{-12}, \end{aligned} \tag{12}$$

and the hadronic light-by-light-scattering (l-l) term is given in Ref. [40]:

$$a_e(\text{had. } l\text{-}l) = 0.035\ (10) \times 10^{-12}. \tag{13}$$

The electroweak contribution has been obtained from the analytic form of the one-loop [41] and two-loop [42–44] electroweak effects on the muon $g-2$, adapted for the electron. We quote the value summarized and updated in Ref. [4]:

$$a_e(\text{electroweak}) = 0.0297\ (5) \times 10^{-12}. \tag{14}$$

To compare the theoretical prediction with the measurement (1), we need the value of the fine-structure constant α determined by a method independent of $g-2$. The best α available at present is the one derived from the precise value of h/m_{Rb}, which is obtained by the measurement of the recoil velocity of Rubidium atoms on an optical lattice [45], combined with the very precisely known Rydberg constant and m_{Rb}/m_e [4]:

$$\alpha^{-1}(\text{Rb10}) = 137.035\ 999\ 049\ (90) \quad [0.66\ \text{ppb}]. \tag{15}$$

With this α the theoretical prediction of a_e becomes

$$a_e(\text{theory}) = 1\ 159\ 652\ 181.643\ (25)(23)(16)(763) \times 10^{-12}, \tag{16}$$

where the first, second, third, and fourth uncertainties come from the eighth-order term (7), the tenth-order term (9), the hadronic (12), (13) and electroweak (14) corrections, and the fine-structure constant (15), respectively. This is in good agreement with the experiment (1):

$$a_e(\text{HV08}) - a_e(\text{theory}) = -0.91\ (0.82) \times 10^{-12}. \tag{17}$$

The intrinsic theoretical uncertainty ($\sim 38 \times 10^{-15}$) of a_e(theory) is less than 1/20 of the uncertainty due to the fine-structure constant (15). This means that α determined

assuming that QED and the standard model are valid and solving the equation a_e(theory) = a_e(experiment) for α gives a value more precise than (15):

$$\alpha^{-1}(a_e) = 137.035\ 999\ 1570\ (29)(27)(18)(331) \quad [0.25\ \text{ppb}], \tag{18}$$

where the uncertainties are from the QED terms (7), (9), combined hadronic (12), (13) and electroweak (14) terms, and the measurement (1) of a_e(HV08), in that order. This provides a stringent constraint on possible theories beyond the standard model. It can be made even more stringent by improved measurements of a_e.

Section II describes how we organized diagrams of Set V into a smaller number of independent integrals. Section III describes the steps involved in the automatic code generation by GENCODE*N*. Section IV discusses computational problems encountered in the numerical integration.

Appendix A describes how *K*-operation, *R*-subtraction and *I*-operation [22, 23, 46] introduced in Section III work, choosing the diagram X253 as an example. Actually X253 is one of the exceptional diagrams (the other is X256) for which the implementation of *I*-operation in GENCODE*N* requires slight modification according to the definition of the residual part of vertex renormalization constant with insertion of a two-point vertex $L^{\rm R}_{n^*}$, which has been treated manually. This is manifested first at these two diagrams in 10th order, while it is absent in the 8th and lower order diagrams. Thus, the evaluation of the 8th order diagrams (called Group V) that relies on GENCODE*N* is correct. The detail will be fully discussed. Appendix B describes our approach to summing up of the residual renormalization terms of Set V.

II. REDUCING THE NUMBER OF INTEGRALS

Our evaluation of the 10th-order diagrams of Set V relies on the numerical integration. The combined uncertainty σ_N of N independent integrals grows roughly as $\sqrt{N}$. Thus σ_N becomes large for large N even if each integral has a small uncertainty. This can be a particularly big headache for the Set V, for which $N = 6354$.

It is thus important to reduce the number of independent integrals as much as possible. For this purpose the technique based on the Ward-Takahashi identity developed previously [46] is found to be handy. It is based on the observation that a set of nine vertex diagrams,

which are derived from the self-energy-like diagram $\mathcal{G}$ of Fig. 1 as the coefficients of terms linear in the external magnetic field, share features which enable us to combine them into a single integral. Let $\Lambda^\nu(p,q)$ be the sum of these nine vertex diagrams, where $p-q/2$ and $p+q/2$ are the 4-momenta of incoming and outgoing lepton lines and $(p-q/2)^2 = (p+q/2)^2 = m^2$. The number of such sums is $6354/9 = 706$. By taking time-reversal symmetry into account, the total number of independent integrals is reduced further to 389. This is still large but far more manageable.

Let $\Sigma(p)$ be the integral representing the self-energy part of a diagram $\mathcal{G}$ of Fig. 1 (namely the part independent of the magnetic field). With the help of the Ward-Takahashi identity, we can rewrite $\Lambda^\nu(p,q)$ as

$$\Lambda^\nu(p,q) \simeq -q_\mu \left[\frac{\partial \Lambda_\mu(p,q)}{\partial q_\nu}\right]_{q=0} - \frac{\partial \Sigma(p)}{\partial p_\nu} \tag{19}$$

in the small q limit. The $g-2$ term $M_{\mathcal{G}}$ is projected out from either the left-hand side (*lhs*) or the right-hand side (*rhs*) of Eq. (19). Considerable numerical cancellation is expected among the nine terms on the *lhs* of Eq. (19). In fact the *rhs* exhibits the consequence of such a cancellation at the algebraic level. Thus starting from the *rhs* enables us to reduce the amount of computing time substantially (by ~ 5), and also to improve the precision of numerical results significantly.

Since these integrals have UV-divergent subdiagrams, they must be regularized by some means. For the diagrams of Set V the Feynman cut-off, which is a sort of "mass" of virtual photons, works fine as the regulator. Suppose all integrals, including renormalization terms, are initially regularized by the Feynman cut-off. Of course the final renormalized result is finite and well-defined in the limit of infinite cut-off mass.

III. FORMULATION

Most of these diagrams are so huge and complicated that numerical integration is the only viable option at present. In order to evaluate them on a computer which requires that every step of computation is finite, however, it is necessary to remove all sources of divergence of the integrand *before* carrying out integration. This is achieved by the introduction of K-operation which deals with the UV divergences [22, 46], and R-subtraction and I-operation which deal with the IR divergences [23, 46]. See III D and III E for more details.

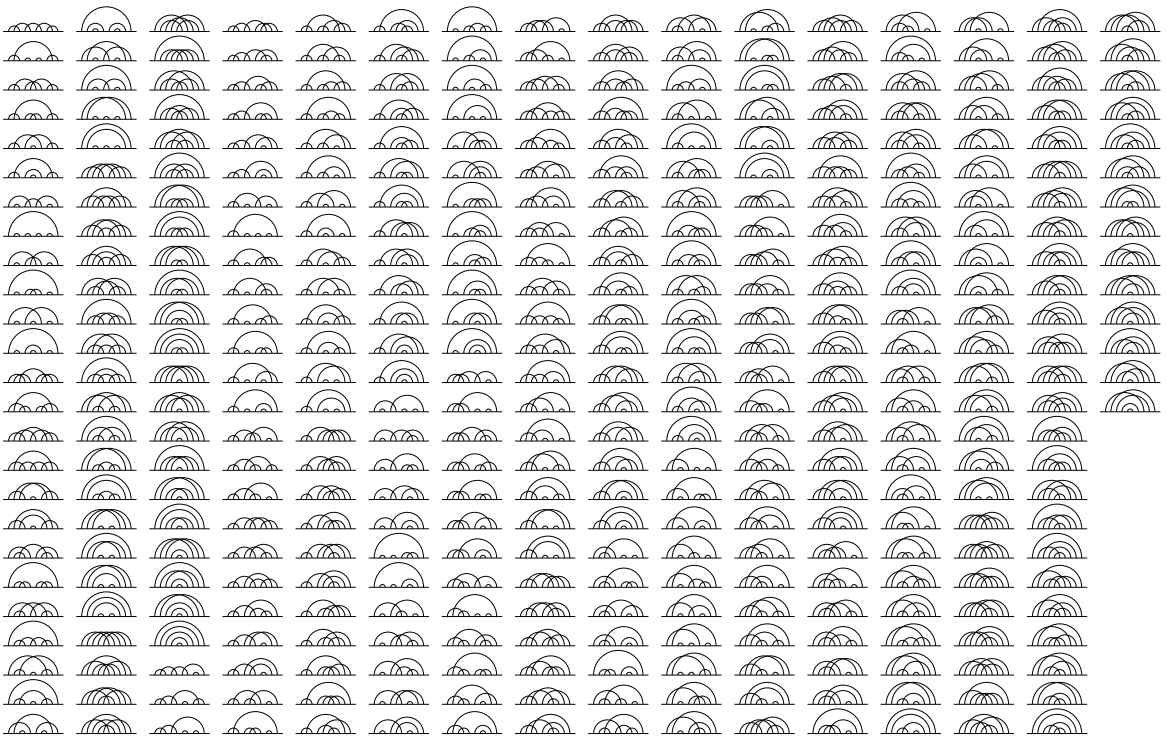

FIG. 1: Overview of 389 diagrams which represents 6354 vertex diagrams of Set V. The horizontal solid lines represent the electron propagators in a constant weak magnetic field. Semi-circles stand for photon propagators. The left-most figures are denoted as X001–X025 from the top to the bottom. The top figure second from the left is denoted X026, and so on.

In practice it is very difficult to carry out such a calculation without making mistakes because of the gigantic size of the integral and a large number of terms required for renormalization. To deal with this problem we developed an automatic code-generating algorithm GENCODEN [22, 23], in which N implies that it works for the q-type diagrams of any order N in the perturbation theory of QED.

A. Diagram Generation

The Feynman diagrams of Set V have the structure that ten vertices along the electron line are connected by the virtual photons a, b, c, d, e, and thus specified by the pairing patterns of how these vertices are connected. Excluding patterns which are not one-particle irreducible, and taking time-reversal invariance into account, we obtain 389 different patterns which are

represented by the diagrams of Fig. 1. They are named as Xnnn, $nnn = 001, 002, \ldots, 389$.

The diagram X001 represents the diagram at the upper left corner of Fig. 1. Subsequent expressions represent diagrams placed below X001 until X025, and X026 corresponds to the diagram placed to the right of X001, and so on. Diagrams X001 to X072 are time-reversal symmetric and diagrams X073 to X389 are asymmetric. Within each group they are arranged in a lexicographical order.

Each of these patterns can be expressed by a "one-line" statement of an ordered sequence of ten vertices labelled by the attached photon line indices. The diagram X001 is identified by the sequence of paring pattern *abacbdcede*, which means that the first and third vertices from the left end of the electron line are connected by the virtual photon a, the second and fifth vertices are connected by the virtual photon b, and so on.

All Feynman diagrams of Set V have a common feature except for the pattern of pairing of vertices. The integral of Set V can thus be generated from a single master code by providing the simple diagram-specific information Xnnn as the input. It is important to note that this pairing pattern not only specifies completely the structure of the unrenormalized diagram but also represents the structure of all UV-divergent and IR-divergent subdiagrams required for renormalization.

B. Construction of unrenormalized integral

From a one-line statement specifying the diagram $\mathcal{G} \equiv$ Xnnn, the *rhs* of Eq. (19) is translated into a momentum space integral applying the Feynman-Dyson rule (assuming the Feynman cutoff). Introducing Feynman parameters z_1, z_2, ..., z_9 for the electron propagators, where z_i is for the i-th electron line from the left end of the diagram, and z_a, z_b, z_c, z_d, z_e for the photon propagators, it carries out the momentum integration *exactly* using a home-made table written in FORM [47]. This leads to an integral of the form

$$M_{\mathcal{G}} = \left(\frac{-1}{4}\right)^5 4! \int (dz)_{\mathcal{G}} \left[\frac{1}{4}\left(\frac{E_0 + C_0}{U^2V^4} + \frac{E_1 + C_1}{U^3V^3} + \ldots\right) + \left(\frac{N_0 + Z_0}{U^2V^5} + \frac{N_1 + Z_1}{U^3V^4} + \ldots\right)\right], \tag{20}$$

where E_n, C_n, N_n and Z_n are functions of Feynman parameters z_i and "symbolic" building blocks A_i, B_{ij}, C_{ij} for electron lines $i, j = 1, 2, \ldots, 9$. n is the number of *contractions* (see Refs. [46, 48] for definitions). See, for example, Ref. [22] for definitions of B_{ij} and C_{ij}. U is the Jacobian of transformation from the momentum variables to Feynman parameters.

$(dz)_{\mathcal{G}}$ is defined by

$$(dz)_{\mathcal{G}} = \prod_{k\in\mathcal{G}} dz_k \; \delta\left(1 - \sum_{k\in\mathcal{G}} z_k\right). \tag{21}$$

A_i is the *scalar current*, which satisfies an analogue of Kirchhoff's laws for electric current, and has the form

$$A_i = \frac{1}{U}\sum_{j=1}^{9}(\delta_{ij}U - z_j B_{ij}). \tag{22}$$

V is obtained by combining all denominators of propagators into one with the help of the Feynman parameters. It has a form common to all diagrams of Fig. 1:

$$V = \sum_{i=1}^{9} z_i(1 - A_i)m^2 + \sum_{\kappa=a}^{e} z_\kappa \lambda^2, \tag{23}$$

where m and λ are rest masses of electron and photon, respectively. Of course, λ must be sent to 0 in the end.

The explicit forms of U and B_{ij} as functions of Feynman parameters depend on the structure of the diagram $\mathcal{G}$. Once they are determined, A_i and V have common expression for all diagrams of Set V. The individual integral is denoted as $M_{\mathcal{G}}$ and the sum of all $M_{\mathcal{G}}$ in Set V is denoted as M_{10}.

C. Construction of building blocks

The conversion of momentum integral into that of Feynman parameters involves inversion of a large matrix, which is performed by MAPLE. This enables us to obtain explicit forms of A_i, B_{ij}, C_{ij}, U as homogeneous functions of $z_1, z_2, \ldots, z_9; z_a, z_b, \ldots, z_e$. V has a form given in Eq. (23) which is common to all diagrams of Set V.

D. Construction of UV divergence subtraction terms

The renormalization of UV divergence is carried out by a subtractive method. A UV divergence of a diagram of Set V arises from a subdiagram $\mathcal{S}$, which is of vertex type or self-energy type. The Set V has no subdiagrams of vacuum-polarization type or light-by-light-scattering type.

Suppose $M_{\mathcal{G}}$ diverges when all loop momenta of a subdiagram $\mathcal{S}$ consisting of $N_{\mathcal{S}}$ lines and $n_{\mathcal{S}}$ closed loops go to infinity. In the Feynman-parametric formulation, this corresponds

to the vanishing of the denominator U when all $z_i \in \mathcal{S}$ vanish simultaneously. To find a criterion for a UV divergence from $\mathcal{S}$, consider the part of the integration domain where z_i satisfies $\sum_{i\in\mathcal{S}} z_i \leq \epsilon$. In the limit $\epsilon \to 0$ one finds

$$\begin{aligned} V &= \mathcal{O}(1), \quad U = \mathcal{O}(\epsilon^{n_{\mathcal{S}}}), \\ B_{ij} &= \mathcal{O}(\epsilon^{n_{\mathcal{S}}-1}) \quad \text{if} \quad i,j \in \mathcal{S}, \\ B_{ij} &= \mathcal{O}(\epsilon^{n_{\mathcal{S}}}) \quad \text{otherwise.} \end{aligned} \tag{24}$$

From this we can obtain a simple UV power-counting rule for identifying UV divergent terms. Based on this information we can construct an integral which has the same UV divergence as $M_{\mathcal{G}}$ but has features suitable as the UV divergence counter term. The K-operation $\mathbb{K}_{\mathcal{S}}$ [22, 46] on $M_{\mathcal{G}}$ that creates such a counter term has properties summarized as follows:

(i) The integral $\mathbb{K}_{\mathcal{S}} M_{\mathcal{G}}$ subtracts the UV divergence arising from the subdiagram $\mathcal{S}$ of $M_{\mathcal{G}}$ *point by point* in the same Feynman parametric space.

(ii) By construction the subtraction term factorizes into pieces of magnetic moments and renormalization constants of lower-order, which are known from lower-order calculation.

For a vertex-type subdiagram $\mathcal{S}$ the K-operation $\mathbb{K}_{\mathcal{S}}$ on $M_{\mathcal{G}}$ factorizes exactly into the product of lower-order quantities as

$$\mathbb{K}_{\mathcal{S}} M_{\mathcal{G}} = L_{\mathcal{S}}^{UV} M_{\mathcal{G}/\mathcal{S}}. \tag{25}$$

where $\mathcal{G}/\mathcal{S}$ is the reduced diagram obtained by shrinking $\mathcal{S}$ in $\mathcal{G}$ to a point, and $L_{\mathcal{S}}^{UV}$ is the leading UV divergent part of the vertex renormalization constant $L_{\mathcal{S}}$.

For a self-energy-type subdiagram $\mathcal{S}$, connected to the rest of $\mathcal{G}$ by electron lines i and j, the K-operation $\mathbb{K}_{\mathcal{S}}$ on $M_{\mathcal{G}}$ gives two terms of the form

$$\mathbb{K}_{\mathcal{S}} M_{\mathcal{G}} = dm_{\mathcal{S}}^{UV} M_{\mathcal{G}/\mathcal{S}(i^*)} + B_{\mathcal{S}}^{UV} M_{\mathcal{G}/[\mathcal{S},j]}. \tag{26}$$

Here $M_{\mathcal{G}/\mathcal{S}(i^*)}$ is the reduced diagram obtained by shrinking $\mathcal{S}$ to a point and i^* indicates that the two-point mass vertex is inserted in the line i of the diagram $M_{\mathcal{G}/\mathcal{S}}$. The second term comes from the diagram obtained by shrinking both $\mathcal{S}$ and j to a point. This term, which is written as $\mathcal{G}/[\mathcal{S},j]$, where $[\mathcal{S},j]$ denotes the sum of two sets, can be transformed into a more convenient form by integration by part with respect to z_i. $dm_{\mathcal{S}}^{UV}$ and $B_{\mathcal{S}}^{UV}$ are the leading UV divergent parts of the mass renormalization constant $dm_{\mathcal{S}}$ and wave-function renormalization constant $B_{\mathcal{S}}$. See Ref. [48] for more details.

(iii) The K-operation generates only the leading UV-divergent parts of renormalization constants. Thus an additional *finite* renormalization (called residual renormalization) is required to recover the standard on-shell renormalization.

In general the subtracting integrand is derived from the original integrand by applying several K-operations on the Zimmermann's forest of subdiagrams [49]. Suppose $\mathbb{K}_{\mathcal{S}}$ is the K-operator associated with a subdiagram $\mathcal{S}$ of a diagram $\mathcal{G}$. Then the UV-finite amplitude $M_{\mathcal{G}}^{\rm R}$ is obtained from the unrenormalized amplitude $M_{\mathcal{G}}$ by the forest formula of the form [22]

$$M_{\mathcal{G}}^{\rm R} = \sum_{f\in\mathfrak{F}(\mathcal{G})} \left[\prod_{S_i\in f} (-\mathbb{K}_{S_i})\right] M_{\mathcal{G}}, \tag{27}$$

where the sum is taken over all forests f, including an empty forest, of the diagram $\mathcal{G}$. The order of operation in the product is arranged so that operations for the outer subdiagrams are applied first.

E. Construction of IR divergence subtraction terms

The IR divergence has its origin in the singularity caused by vanishing mass of virtual photon. However, this is just a necessary condition, not a sufficient condition. In order that this singularity causes actual IR divergence of the integral it must be enhanced by vanishing of denominators of two or more electron propagators (called *enhancers*) due to kinematic constraints. Such a situation arises in the diagrams that have self-energy subdiagrams. It is associated with the vanishing of V-function of the denominators in Eq. (20) in the integration domain characterized by [46, 48]

$$\begin{aligned}
&z_i = \mathcal{O}(\delta) && \text{if } i \text{ is an electron line in } \mathcal{R}, \text{ where } \mathcal{R}\equiv\mathcal{G}/\mathcal{S},\\
&z_i = \mathcal{O}(1) && \text{if } i \text{ is a photon line in } \mathcal{R},\\
&z_i = \mathcal{O}(\epsilon),\ \epsilon\sim\delta^2, && \text{if } i\in\mathcal{S}.
\end{aligned} \tag{28}$$

The origin of linear or higher power IR-divergence is easy to identify diagrammatically. It is caused when the diagram has two or more disconnected self-energy-like subdiagrams and one of the self-energy-like subdiagrams behaves as a self-mass when the photon momenta of the diagram outside the self-energy-like subdiagram vanish and the electron lines attached to it go on shell.

Our treatment of self-energy subdiagram by means of the K-operation subtracts only the UV-divergent part of the self-mass as is shown in Eq. (26). The unsubtracted remainder of self-mass term is proportional to $M_{\mathcal{G}/\mathcal{S}(i^*)}$, which contains an IR divergence. (In the case of second-order self-mass this problem does not arise since the entire self-mass term is removed by the K-operation.)

In order to avoid this problem we developed a method, called R-subtraction [50], which removes the finite remnant of the self-mass term completely, wherever it arises in a diagram. For a formal treatment, we introduce the R-subtraction operator $\mathbb{R}_{\mathcal{S}}$

$$\mathbb{R}_{\mathcal{S}} M_{\mathcal{G}} = dm^{\mathrm{R}}_{\mathcal{S}} M^{\mathrm{R}}_{\mathcal{G}/\mathcal{S}\,(i^\star)}, \tag{29}$$

where $dm^{\mathrm{R}}_{\mathcal{S}}$ is the UV-finite part of the mass renormalization constant defined by

$$dm^{\mathrm{R}}_{\mathcal{S}} = dm_{\mathcal{S}} - dm^{\mathrm{UV}}_{\mathcal{S}} + \sum_f \prod_{\mathcal{S}'\in f} (-\mathbb{K}_{\mathcal{S}'})\, \widetilde{dm}_{\mathcal{S}}, \tag{30}$$

and $M^{\mathrm{R}}_{\mathcal{G}/\mathcal{S}\,(i^\star)}$ is the UV-finite part extracted by means of the K-operation on the magnetic moment amplitude of the residual diagram $\mathcal{G}/\mathcal{S}$

$$M^{\mathrm{R}}_{\mathcal{G}/\mathcal{S}\,(i^\star)} = \sum_f \prod_{\mathcal{S}'\in f} (-\mathbb{K}_{\mathcal{S}'})\, M_{\mathcal{G}/\mathcal{S}\,(i^\star)}, \tag{31}$$

in which the leading UV-divergent part $dm^{\mathrm{UV}}_{\mathcal{S}}$ is entirely removed from the renormalization constant $dm_{\mathcal{S}}$ and the UV divergence in the remainder $\widetilde{dm} \equiv dm - dm^{\mathrm{UV}}$ is subtracted away by applying the K-operation associated with the forest f.

The R-subtraction removes the power-law IR divergences as well as logarithmic divergences related to self-mass. Another type of logarithmic IR divergence occurs, however, when the self-energy-like subdiagram $\mathcal{S}$ behaves as a lower-order magnetic moment and the residual factor $\mathcal{G}/\mathcal{S}$ contains an IR singularity analogous to the vertex renormalization constant of the diagram $\mathcal{G}/\mathcal{S}$.

By construction the resulting integral is factorizable into the product of the magnetic moment $M_{\mathcal{S}}$ defined on the subset $\mathcal{S}$ and the UV-finite part $L^{\mathrm{R}}_{\mathcal{G}/\mathcal{S}}$ of the vertex renormalization constant $L_{\mathcal{G}/\mathcal{S}}$ defined by

$$L^{\mathrm{R}}_{\mathcal{G}/\mathcal{S}} = L_{\mathcal{G}/\mathcal{S}} - L^{\mathrm{UV}}_{\mathcal{G}/\mathcal{S}} + \sum_f \prod_{\mathcal{S}'\in f} (-\mathbb{K}_{\mathcal{S}'})\, \widetilde{L}_{\mathcal{G}/\mathcal{S}}, \tag{32}$$

in which the leading UV-divergent part $L^{\mathrm{UV}}_{\mathcal{G}/\mathcal{S}}$ and the UV-divergent parts associated with the forests $\prod_{\mathcal{S}'\in f} (-\mathbb{K}_{\mathcal{S}'})\, \widetilde{L}_{\mathcal{G}/\mathcal{S}}$ are subtracted away, where $\widetilde{L} \equiv L - L^{\mathrm{UV}}$.

The I-subtraction operator $\mathbb{I}_{\mathcal{S}}$ acting on the unrenormalized amplitude $M_{\mathcal{G}}$ is defined by

$$\mathbb{I}_{\mathcal{S}} M_{\mathcal{G}} = L^{\mathrm{R}}_{\mathcal{G}/\mathcal{S}} M^{\mathrm{R}}_{\mathcal{S}}. \tag{33}$$

N. B. The IR power counting rule identifies only IR-divergent part. It does not specify how to handle the IR-finite part. The I-subtraction operation defined by Eq. (33) handles the IR-finite terms in a manner different from that of the old subtraction method [46, 48]. Note also that the "new" I-subtraction operation applies only to the self-energy-like subdiagram $\mathcal{S}$.

The whole set of IR subtraction terms can be obtained by the combination of R- and I-operations, both of which belong to *annotated forests* [23]. An annotated forest is a set of self-energy-like subdiagrams, to each element of which the distinct operation of I-subtraction or R-subtraction is assigned. The IR-subtraction term associated with an annotated forest is constructed by successively applying operators $\mathbb{I}$ or $\mathbb{R}$, and takes the form

$$(-\mathbb{I}_{\mathcal{S}_i}) \ldots (-\mathbb{R}_{\mathcal{S}_j}) \ldots M_{\mathcal{G}} \tag{34}$$

where the annotated forest consists of the subdiagrams $\mathcal{S}_i, \ldots$ and $\mathcal{S}_j, \ldots$.

F. Residual renormalization

The output of the steps **A** through **E** which has been made UV-finite by K-operation and IR-finite by R- and I-operations, is not the standard-renormalized integral. Thus an additional finite renormalization is required to obtain the standard result of on-shell-renormalization.

The sum of residual renormalization terms of all diagrams of Set V is shown in Appendix B. The result can be written as the sum of terms, all of which are free from UV-

and IR-divergences:

$$
\begin{aligned}
A_1^{(10)}[\text{Set V}] &= \Delta M_{10}[\text{Set V}] \\
&\quad + \Delta M_8(-7\Delta LB_2) \\
&\quad + \Delta M_6\{-5\Delta LB_4 + 20(\Delta LB_2)^2\} \\
&\quad + \Delta M_4\{-3\Delta LB_6 + 24\Delta LB_4\Delta LB_2 - 28(\Delta LB_2)^3 + 2\Delta L_{2^*}\Delta dm_4\} \\
&\quad + M_2\{-\Delta LB_8 + 8\Delta LB_6\Delta LB_2 - 28\Delta LB_4(\Delta LB_2)^2 \\
&\qquad + 4(\Delta LB_4)^2 + 14(\Delta LB_2)^4 + 2\Delta dm_6\Delta L_{2^*}\} \\
&\quad + M_2\Delta dm_4(-16\Delta L_{2^*}\Delta LB_2 + \Delta L_{4^*} - 2\Delta L_{2^*}\Delta dm_{2^*}),
\end{aligned}
\tag{35}
$$

where ΔM_n, ΔLB_n, Δdm_n, ΔL_{n^*}, and Δdm_{2^*} are finite quantities of lower orders obtained in our calculation of lower order a_e. (All these are quantities of q-type diagrams since subdiagrams of Set V are all q-type.) See Appendix B for precise definitions.

IV. NUMERICAL INTEGRATION

We evaluate individual integrals by numerical integration using the iterative-adaptive Monte-Carlo routine VEGAS [10]. A typical integrand consists of about 90,000 lines of FORTRAN codes occupying more than 6 Megabytes. The domain of integration is a 13-dimensional unit cube ($0 \le x_i \le 1,\ i = 1, 2, \ldots, 13$) onto which the hyperplane of 14 Feynman parameters (see Eq. (21)) is mapped.

In order to assure the credibility of results it is important to understand the nature of error estimate generated by VEGAS. An important feature of VEGAS is that its sampling points of the integrand tend to accumulate after several iterations in the region where it gives the most contribution to the integral. Errors encountered in our work arise primarily from the following three features of our integrands:

(a) Our integrands are singular on some boundary surface of the unit cube because of vanishing of the denominators U and/or V, whether they are renormalized or not.

(b) Our renormalization is performed numerically on a computer, which means mutual cancellation of ∞'s at every singular point in the domain of integration.

(c) The sheer size of the integrands makes it difficult to accumulate a sufficient amount of sampling data with limited computing power available.

A. Steep landscape of integrands and stretching

At first sight, the feature (a) seems to indicate that it is hopeless to obtain a reliable result for such a singular integrand. However, the measure of immediate neighborhood of singularity is small enough so that the integral itself is well defined and convergent because of renormalization.

Nevertheless, steep landscape of the integrand may be a cause for concern since the grid adjustment by VEGAS might not reach the optimal stage as rapidly as one would wish. This problem may be alleviated, however, by "stretching" the integration variables. (See Sec. 6.3 of Ref. [48].)

Suppose VEGAS finds after several iterations that sampling points are highly concentrated at one end of the integration domain, say $x_i = 0$, where x_i is one of the axes of the hypercube. In such a case, if one maps x_i into x_i' as

$$x_i = x_i'^{a_i}, \tag{36}$$

where a_i is some real number greater than 1, the neighborhood of $x_i = 0$ is stretched out and random samplings in x_i' gives more attention to the region near $x_i = 0$ from the beginning of iteration. Also the Jacobian $a_i x_i'^{a_i - 1}$ of the transformation (36) has the effect of reducing the peak of the integrand. Similarly, the singularity at $x_i = 1$ can be weakened by the stretching

$$x_i = 1 - (1 - x_i')^{b_i}, \tag{37}$$

where b_i is some real number greater than 1.

Stretching may be applied to all integration variables independently. By an appropriate choice of parameters a_1, a_2,... and b_1, b_2,... the convergence of iteration can be accelerated considerably.

Note that the stretching is not an attempt to simulate the integrand itself. It is designed to reduce the size of peaks indicated by preceding iterations so that the sampling points become more evenly distributed throughout the transformed domain of integration. It is easy to implement since it is applied to each axis independently. Since there is no constraint on the choice of a_i and b_i, except that they must be real numbers larger than 1, one can try various stretches and choose more efficient one. Since different stretches are nothing but evaluation of the same integral with different distributions of sampling points, they can also

be used to check the consistency of calculation.

B. Extended numerical precision

Concerning the feature (b), the integrals are made convergent by point-by-point cancellation of divergences by carefully tailored counter-terms created by the intermediate renormalization procedure. All this would pose no problem if each step of computation were carried out with infinite precision. In practice, however, we have to perform calculations in finite precision. The intended cancellation may fail occasionally because cancelling terms have only finite number of significant digits, and their difference, which is supposed to vanish at the singular point, might be dominated near the singularity by roundoff errors, causing uncontrolled fluctuation. This problem can be reduced to a manageable level by adopting higher precision arithmetics which will reduce the size of dangerous integration volume, although it slows down the computation severely.

In our calculation, a part of diagrams are evaluated in the double-double (pseudo-quadruple) precision arithmetic using the library written by one of us which is the arrayed version of the algorithm presented in qd library [51]. For a diagram that exhibits even more severe digit-deficiency, $X008$, the most singular part of the integral is evaluated with quadruple-double (pseudo-octuple) precision and the remaining part is evaluated with the double-double precision.

C. Intensive computation

The feature (c), huge size of our integrands, means that they require a large amount of computing time in order to accumulate sufficient sampling statistics. Indeed, this combined with the difficulty in accessing adequate computing resources has been the main cause of delay in obtaining high accuracy result thus far.

D. Numerical integration process and the result

All integrals are evaluated initially in double precision using 10^7 sampling points per iteration, iterated 50 times, followed by 10^8 points per iteration, iterated 50 times. This

step is to confirm that our renormalization scheme actually works and gives finite results.

The output of GENCODEN, being a universal code, employes a generic mapping of the Feynman parameters (denoted as the default mapping), and is not optimized for the individual diagrams.

The first thing we must do to improve the convergence of iteration is to note that diagrams containing n_s subdiagrams of self-energy type require only $(13-n_s)$ independent integration variables. The reduction of integration variables helps improve the convergence of VEGAS iterations. We shall call the class of these diagrams XB. It consists of 236 diagrams. The remainder, which consists of 153 diagrams without self-energy subdiagram, will be called XL.

Another improvement takes account of the fact that the iteration of VEGAS converges better if singular behavior of the integrand is confined to one axis. For instance we may choose the largest sum of Feynman parameters that vanishes at the singularity of the integrand as one to be mapped onto an integration variable. See discussion around Eq. (24). This is not always possible for our integrands which may have multiple sets of singular axes, but it still helps.

After these adjustments are made, each integral is evaluated in double precision arithmetic with 10^9 sampling points, which takes 1 to 3 hours on 32 cores of RICC (RIKEN Integrated Clusters of Clusters). Evaluation in double-double (pseudo-quadruple) precision is about 60 times slower. Some large runs in double-double precision with 10^9 sampling points per iteration, iterated 80 times, took about 65 days on the 128 cores of RICC.

Thus far XL-integrals were evaluated in two ways:

1) Primary runs with the default mapping in double precision arithmetic. [$XL1$]

2) Second runs with the adjusted mapping in double precision arithmetic. [$XL2$]

XB-integrals were evaluated in three ways:

1) Primary runs with the default mapping in double precision arithmetic. [$XB1$]

2a) Second run with the adjusted mapping in double-double precision arithmetic. There are 162 integrals. [$XB2$a]

2b) Remaining 74 integrals evaluated after the preliminary result was published. [$XB2$b]

3) Third run in double precision for 176 of 236 integrals, and double-double precision for the remaining 60 integrals. [$XB3$]

By early 2012 we managed to reduce the uncertainties of all individual integrals to less than 0.05. The value of $A_1^{(10)}$[Set V] was obtained by combining $XL1$, $XB1$, and $XB2a$. The combined uncertainty of $A_1^{(10)}$[Set V] was about 0.57. This was reported as a very preliminary value: [9]

$$A_1^{(10)}[\text{Old Set V}] = 10.092\ (570). \tag{38}$$

Since the preliminary result was published, we have reevaluated all tenth-order integrals for various choices of mapping. The new result consists of $XL2$, $XB2a$, $XB2b$, and $XB3$, excluding $XL1$ and $XB1$. They are summarized in Table I. Auxiliary quantities required for the residual renormalization are listed in Table II. Combining them all we obtain

$$A_1^{(10)}[\text{Set V}] = 8.726\ (336). \tag{39}$$

The difference of new and old results is 1.366, which is twice as large as the combined uncertainty 0.662. Another point to notice is that, in spite of the far greater numbers of sampling points, the uncertainty of (39) is only 1.7 times smaller than the uncertainty of the very preliminary result (38).

E. Remarks

In order to understand the possible cause of these results it is necessary to examine the behavior of individual integrals. VEGAS subdivides the integration domain into *grid*, from which sampling points of integrand are taken. The grid is adjusted adaptively based on the results of previous iterations so that the importance sampling is achieved. If the absolute value of the integrand has a peak, sampling points will accumulate in that neighborhood as the iteration progresses to accelerate the convergence.

For the multivariate integration, the grid adjustment relies on the profile of the integral projected along each axis. It is monitored by the information that VEGAS provides after each iteration by printing out the values of the integrand at ten points along each axis integrated over the remaining variables, in addition to the value and error of the integral itself. However, some integrands may have several competing peaks. In such a case VEGAS

might find initially only one peak, unaware of the presence of other peaks, if the number of sampling points is too small, and might be lead to unstable convergence, a misleading values, or an unreliable error estimate.

It may occur that the grid adjustment does not work well when the peaks or singularities of the integrand are not localized along an axis but rather located, for instance, in the diagonal region over several axes.[1] In our calculation, the singular behavior of the integrand associated with the divergences lies at the boundaries of the integration domain. It should be desirable to choose integration variables so that the singularities are concentrated on one end of the axis, e.g., $x_i \to 0$ rather than the situation where they emerge, e.g., when the variables x_i and x_j go to zero simultaneously.

We may note that 14 Feynman parameters z_i of 10th order diagrams satisfying $\sum z_i = 1$ are mapped to the integration domain of a 13 dimensional unit cube. The choice of mapping is arbitrary, and thus the appropriate mapping should be applied that takes account of the above considerations, reflecting the substructure of the diagram. In general, the default mapping adopted in the output of GENCODEN, being the universal code, is not optimal in this sense.

The calculation runs $XL1$ and $XB1$ contributing to the preliminary result [9] rely on the default mapping. Several integrals seems to suffer from some of the problems described above. By using the different mappings that are tailored for individual diagrams, especially for the diagrams of $XL1$ containing several second-order vertex subdiagrams, the convergence rates of the integral have been much improved and the reliable error estimates are obtained. This observation suggests that in the numerical integration of the 10th order diagrams, when the number of sampling points are not large enough, the inappropriate mapping would lead to some underestimate of the error because the evaluated integrands over the sampling points do not obey the Gaussian distribution. The uncertainty of Ref. [9] was thus not yet reliable and must be enlarged substantially. On the other hand, integrals contributing to the new result behave much better presumably because of the new mappings. The values and the error estimates are reliable also because of substantially increased sampling statistics.

[1] New version of VEGAS provided by P. Lepage in 2013 overcomes this known weakness of the original version of VEGAS [10]. The new VEGAS can be obtained from `https://github.com/gplepage/vegas`. We have not used the new VEGAS algorithm, since it was released after we had carried out most of Set V integration over several years.

Now that the improved values of all diagrams of Set V are obtained we have a complete evaluation of 12,672 diagrams of tenth-order [11–20]. Taking (39) into account we report

$$A_1^{(10)} = 7.795\ (336) \tag{40}$$

as the new tenth-order term. It is about 14 times more precise than the crude estimate $|A_1^{(10)}| < 4.6$ [52] and makes the overall *theoretical* uncertainty about 7.5 times smaller than the current experimental uncertainty [1, 2].

V. DISCUSSION

In view of the enormous size and complexity of the integrals of Set V, it is unlikely that the validity of our results can be tested by an independent method any time soon. We are thus obliged to establish their validity to the best of our capability.

First of all we have to make sure that our formulation is analytically exact. FORTRAN codes of all integrals of Set V are created by the code-generating algorithm GENCODEN, which has been tested extensively by applying it to the creation of lower-order diagrams of q-type. Recall that N of GENCODEN represents the number of vertices of q-type diagrams where virtual photons are attached. For $N = 10$ it generates a complete set of distinct irreducible diagrams of Set V automatically. Similarly, complete sets of distinct q-type diagrams of sixth- or eighth-orders are generated by GENCODEN for $N = 6$ or 8. Since these integrals have been thoroughly tested by comparison with previous formulations, we may expect that GENCODEN works correctly for $N = 10$, too. We have found, however, that the implementation of GENCODEN for constructing some IR-subtraction terms of the diagrams X253 and X256 requires modifications according to the definition of the renormalization constants with two-point vertex insertion. Since these exceptions are minor, we have corrected them manually instead of rewriting GENCODEN itself. This problem and its correction is discussed in full detail in Appendix A. With this modification the FORTRAN codes of 389 integrals, including residual renormalization terms, give a fully renormalized and analytically exact formula of $A_1^{(10)}$ for the Set V.

The only uncertainty of our results thus arises from the numerical integration by the Monte-Carlo integration routine VEGAS [10]. The reliability of VEGAS has been tested thoroughly by applying it to the evaluation of thousands of complicated integrals of sixth-

order and eighth-order. In all these cases the error estimates obtained by VEGAS, based on random sampling of the integrand, are found to be very reliable, provided that a sufficiently large number of sampling data is accumulated. This is helped significantly by stretching. Double-double precision arithmetic is used whenever problem caused by digit deficiency is suspected. Of course because of their gigantic size numerical integration is extremely time-consuming and accumulation of sampling statistics is a slow process. Inspection of Table I suggests that some of the integrals may benefit from more extensive samplings. There is an ongoing effort to improve the sampling statistics.

TABLE I: VEGAS integration results of $X001$–$X389$ of the tenth-order Set V diagrams. The superscript dd in the first column means that the integrand was evaluated with the double-double (pseudo-quadruple) precision. The superscript qd on $X008$ indicates that the most singular part of the integral $X008$ is evaluated with quadruple-double (pseudo-octuple) precision and the remaining part is evaluated with the double-double precision. Other integrals without the superscript were evaluated with the double precision. The second column shows the symbolic representation of the diagram. The third column counts the number of subtraction terms. The fourth column presents the value of the integral with error in the last few digits in the parenthesis. The fifth column lists the total number of iterations evaluated with 10^9 sampling points per iteration.

Diagram	Vertex repr.	No. of subtr. terms	Value (Error) including n_F	No. of iterations with 10^9 sampling points per iteration
$X001$	*abacbdcede*	47	−0.1724 (91)	20
$X002^{dd}$	*abaccddebe*	47	−5.9958 (333)	13
$X003$	*abacdbcede*	19	−0.1057 (52)	10
$X004^{dd}$	*abacdcdebe*	71	5.1027 (339)	9
$X005$	*abacddbece*	43	1.1112 (168)	20
$X006$	*abacddcebe*	59	−5.2908 (245)	9
$X007$	*abbcadceed*	47	−3.4592 (254)	25
$X008^{qd}$	*abbccddeea*	47	−16.5070 (289)	11
$X009$	*abbcdaceed*	19	−3.1069 (71)	24
$X010^{dd}$	*abbcdcdeea*	83	11.2644 (342)	124
$X011^{dd}$	*abbcddaeec*	43	6.0467 (338)	22
$X012^{dd}$	*abbcddceea*	67	−9.3328 (267)	26
$X013$	*abcabdecde*	7	−1.3710 (31)	2
$X014$	*abcacdedbe*	31	0.8727 (42)	10
$X015$	*abcadbecde*	2	2.1090 (8)	2
$X016$	*abcadcedbe*	2	−0.9591 (7)	2
$X017$	*abcaddebce*	6	0.5146 (13)	20
$X018$	*abcaddecbe*	6	0.0309 (13)	20
$X019$	*abcbadeced*	31	1.2965 (48)	10
$X020^{dd}$	*abcbcdedea*	134	−8.1900 (318)	43
$X021$	*abcbdaeced*	11	−0.2948 (15)	10
$X022$	*abcbdcedea*	79	0.8892 (226)	22
$X023$	*abcbddeaec*	27	0.4485 (55)	25
$X024$	*abcbddecea*	75	−6.0902 (246)	23
$X025$	*abccadeebd*	39	−0.7482 (194)	20
$X026^{dd}$	*abccbdeeda*	95	−7.8258 (277)	8
$X027$	*abccdaeebd*	15	−2.3260 (54)	13
$X028^{dd}$	*abccdbeeda*	71	4.5663 (342)	49
$X029^{dd}$	*abccddeeab*	35	6.9002 (233)	1
$X030^{dd}$	*abccddeeba*	67	−12.6225 (342)	34

TABLE I (continued): VEGAS integration results of $X001$–$X389$ of the tenth-order Set V diagrams.

Diagram	Vertex repr.	No. of subtr. terms	Value (Error) including n_F	No. of iterations with 10^9 sampling points per iteration
$X031$	*abcdaebcde*	2	2.3000 (14)	4
$X032$	*abcdaecdbe*	2	−0.2414 (6)	2
$X033$	*abcdaedbce*	2	−1.3806 (7)	2
$X034$	*abcdaedcbe*	2	1.2585 (9)	4
$X035$	*abcdbeaced*	2	−0.5899 (3)	2
$X036$	*abcdbecdea*	11	0.2318 (11)	30
$X037$	*abcdbedaec*	2	−0.7407 (5)	2
$X038$	*abcdbedcea*	11	−0.2927 (14)	20
$X039$	*abcdceaebd*	11	0.3292 (12)	10
$X040$	*abcdcebeda*	47	1.3397 (50)	12
$X041$	*abcdcedeab*	63	3.1076 (94)	25
$X042$	*abcdcedeba*	119	−4.1353 (192)	20
$X043$	*abcddeeabc*	15	−2.9620 (29)	21
$X044^{dd}$	*abcddeebca*	59	4.4121 (281)	4
$X045$	*abcddeecab*	43	3.4331 (212)	20
$X046^{dd}$	*abcddeecba*	95	−7.7564 (339)	15
$X047$	*abcdeabcde*	2	−4.4496 (40)	8
$X048$	*abcdeacdbe*	2	−0.8061 (8)	2
$X049$	*abcdeadbce*	2	−0.0278 (7)	2
$X050$	*abcdeadcbe*	2	−1.2213 (9)	4
$X051$	*abcdebaced*	2	−0.1776 (6)	2
$X052$	*abcdebcdea*	11	1.0293 (17)	20
$X053$	*abcdebdaec*	2	0.3699 (4)	2
$X054$	*abcdebdcea*	11	−0.5174 (11)	20
$X055$	*abcdecaebd*	2	−0.3673 (4)	2
$X056$	*abcdecbeda*	11	−0.2650 (27)	20
$X057$	*abcdecdeab*	23	2.7370 (31)	30
$X058$	*abcdecdeba*	44	−5.2510 (70)	12
$X059$	*abcdedeabc*	23	2.1866 (28)	30
$X060$	*abcdedebca*	92	−3.2089 (188)	22
$X061$	*abcdedecab*	68	−3.7724 (137)	20
$X062$	*abcdedecba*	161	5.9174 (262)	26
$X063$	*abcdeeabcd*	6	3.4295 (14)	20
$X064$	*abcdeeacbd*	6	−0.2772 (8)	20
$X065$	*abcdeebadc*	6	0.1551 (13)	20
$X066$	*abcdeebcda*	26	−3.6145 (45)	21
$X067$	*abcdeecdab*	50	−1.6761 (85)	25
$X068$	*abcdeecdba*	98	2.7855 (217)	22
$X069$	*abcdeedabc*	18	−1.2627 (31)	11
$X070$	*abcdeedbca*	70	3.2149 (144)	20

TABLE I (continued): VEGAS integration results of $X001$–$X389$ of the tenth-order Set V diagrams.

Diagram	Vertex repr.	No. of subtr. terms	Value (Error) including n_F	No. of iterations with 10^9 sampling points per iteration
$X071$	*abcdeedcab*	54	3.7025 (96)	20
$X072$	*abcdeedcba*	134	−5.5704 (208)	15
$X073$	*abacbdceed*	47	3.4114 (254)	24
$X074$	*abacbddece*	47	4.4104 (251)	49
$X075^{dd}$	*abacbddeec*	47	−8.1138 (340)	33
$X076$	*abacbdecde*	19	−5.3405 (74)	26
$X077$	*abacbdeced*	39	3.5459 (86)	56
$X078$	*abacbdedce*	39	1.1666 (80)	56
$X079$	*abacbdedec*	71	5.3956 (305)	41
$X080$	*abacbdeecd*	43	0.4597 (257)	28
$X081$	*abacbdeedc*	59	−5.6566 (248)	26
$X082^{dd}$	*abaccdbeed*	47	−8.5156 (348)	92
$X083^{dd}$	*abaccddeeb*	47	18.7464 (346)	117
$X084$	*abaccdebde*	19	8.9888 (129)	20
$X085$	*abaccdebed*	39	−2.2833 (197)	20
$X086$	*abaccdedbe*	39	0.5180 (223)	20
$X087^{dd}$	*abaccdedeb*	77	−16.5849 (349)	160
$X088^{dd}$	*abaccdeebd*	43	−5.2606 (340)	58
$X089^{dd}$	*abaccdeedb*	63	12.6789 (341)	59
$X090$	*abacdbceed*	19	1.5206 (130)	20
$X091$	*abacdbdece*	39	−1.6355 (97)	56
$X092$	*abacdbdeec*	39	2.1303 (218)	15
$X093$	*abacdbecde*	7	−1.7594 (42)	10
$X094$	*abacdbeced*	15	−1.0419 (66)	10
$X095$	*abacdbedce*	7	0.5838 (35)	6
$X096$	*abacdbedec*	31	1.3458 (73)	10
$X097$	*abacdbeecd*	17	5.0319 (89)	24
$X098$	*abacdbeedc*	33	−1.9806 (183)	20
$X099$	*abacdcbeed*	39	3.0771 (187)	20
$X100^{dd}$	*abacdcdeeb*	77	−15.2919 (331)	244
$X101$	*abacdcebde*	15	−0.2462 (64)	12
$X102$	*abacdcebed*	31	−1.2883 (75)	26
$X103$	*abacdcedbe*	31	0.9424 (74)	10
$X104$	*abacdcedeb*	79	6.4131 (298)	42
$X105$	*abacdceebd*	35	3.0503 (215)	21
$X106$	*abacdceedb*	71	−11.5662 (344)	48
$X107^{dd}$	*abacddbeec*	43	−4.6573 (345)	77
$X108^{dd}$	*abacddceeb*	63	12.9775 (341)	58
$X109$	*abacddebce*	17	−0.0860 (85)	25
$X110$	*abacddebec*	35	1.9248 (204)	20

TABLE I (continued): VEGAS integration results of $X001$–$X389$ of the tenth-order Set V diagrams.

Diagram	Vertex repr.	No. of subtr. terms	Value (Error) including n_F	No. of iterations with 10^9 sampling points per iteration
$X111$	*abacddecbe*	33	3.3578 (132)	24
$X112$	*abacddeceb*	71	−11.8998 (332)	53
$X113^{dd}$	*abacddeebc*	39	−4.3847 (322)	16
$X114^{dd}$	*abacddeecb*	63	11.0641 (343)	54
$X115$	*abacdebcde*	7	−0.5974 (52)	12
$X116$	*abacdebced*	7	1.8362 (28)	10
$X117$	*abacdebdce*	7	0.3292 (27)	10
$X118$	*abacdebdec*	15	−3.2721 (55)	10
$X119$	*abacdebecd*	15	−0.0751 (53)	10
$X120$	*abacdebedc*	31	1.8769 (72)	10
$X121$	*abacdecbde*	7	−0.8549 (43)	6
$X122$	*abacdecbed*	7	−0.7337 (42)	6
$X123$	*abacdecdbe*	15	−3.3559 (67)	12
$X124$	*abacdecdeb*	29	11.5746 (106)	26
$X125$	*abacdecebd*	31	0.8677 (64)	10
$X126$	*abacdecedb*	59	−1.5696 (162)	26
$X127$	*abacdedbce*	15	1.1412 (46)	10
$X128$	*abacdedbec*	31	0.6493 (59)	10
$X129$	*abacdedcbe*	31	1.4833 (70)	10
$X130$	*abacdedceb*	59	−1.5696 (180)	20
$X131$	*abacdedebc*	59	3.1060 (287)	33
$X132^{dd}$	*abacdedecb*	101	−8.8300 (337)	43
$X133$	*abacdeebcd*	17	2.7263 (88)	24
$X134$	*abacdeebdc*	33	−0.6712 (123)	23
$X135$	*abacdeecbd*	33	0.9256 (153)	22
$X136$	*abacdeecdb*	65	−7.5256 (305)	46
$X137$	*abacdeedbc*	45	−2.3541 (233)	23
$X138$	*abacdeedcb*	85	10.1610 (284)	38
$X139^{dd}$	*abbcaddeec*	47	14.8650 (348)	104
$X140$	*abbcadeced*	39	−2.7901 (206)	21
$X141^{dd}$	*abbcadedec*	74	−12.5567 (350)	261
$X142^{dd}$	*abbcadeecd*	43	−1.5767 (341)	66
$X143^{dd}$	*abbcadeedc*	61	10.3225 (341)	58
$X144^{dd}$	*abbccdedea*	83	23.7239 (368)	230
$X145^{dd}$	*abbccdeeda*	67	−18.6212 (349)	115
$X146^{dd}$	*abbcdadeec*	39	−2.2990 (335)	25
$X147$	*abbcdaeced*	15	1.1243 (55)	20
$X148$	*abbcdaedec*	31	−1.4150 (76)	21
$X149$	*abbcdaeecd*	17	−8.3898 (139)	19
$X150^{dd}$	*abbcdaeedc*	33	2.8758 (260)	2

TABLE I (continued): VEGAS integration results of $X001$–$X389$ of the tenth-order Set V diagrams.

Diagram	Vertex repr.	No. of subtr. terms	Value (Error) including n_F	No. of iterations with 10^9 sampling points per iteration
$X151^{dd}$	*abbcdcedea*	87	−10.9362 (344)	68
$X152^{dd}$	*abbcdceeda*	77	14.6793 (345)	113
$X153^{dd}$	*abbcddecea*	77	14.8936 (343)	80
$X154^{dd}$	*abbcddeeca*	67	−20.6285 (342)	90
$X155$	*abbcdeadec*	15	5.0341 (46)	20
$X156$	*abbcdeaedc*	31	−0.8277 (69)	14
$X157$	*abbcdecdea*	32	−11.8490 (252)	18
$X158^{dd}$	*abbcdeceda*	65	0.4607 (329)	6
$X159$	*abbcdedcea*	65	0.4435 (351)	27
$X160^{dd}$	*abbcdedeca*	116	14.0724 (349)	176
$X161^{dd}$	*abbcdeecda*	71	7.8073 (342)	68
$X162^{dd}$	*abbcdeedca*	95	−12.8293 (339)	43
$X163$	*abcabdceed*	19	6.8168 (202)	21
$X164^{dd}$	*abcabddeec*	19	−12.8880 (208)	3
$X165$	*abcabdeced*	15	−2.1661 (76)	10
$X166$	*abcabdedce*	15	−2.3080 (70)	10
$X167$	*abcabdedec*	29	12.1361 (150)	20
$X168$	*abcabdeecd*	17	3.4447 (120)	24
$X169$	*abcabdeedc*	25	−6.9379 (108)	20
$X170$	*abcacdbeed*	39	0.2635 (288)	36
$X171^{dd}$	*abcacddeeb*	39	−2.5229 (313)	7
$X172$	*abcacdebed*	31	1.5601 (76)	26
$X173$	*abcacdedeb*	59	0.0193 (298)	48
$X174$	*abcacdeebd*	35	1.7158 (191)	25
$X175$	*abcacdeedb*	51	−1.8253 (175)	19
$X176$	*abcadbceed*	7	0.7450 (35)	20
$X177$	*abcadbdeec*	15	0.0079 (81)	21
$X178$	*abcadbeced*	5	0.7159 (28)	2
$X179$	*abcadbedce*	2	−0.4377 (8)	4
$X180$	*abcadbedec*	11	0.0284 (25)	4
$X181$	*abcadbeecd*	6	−4.4372 (28)	30
$X182$	*abcadbeedc*	12	1.2822 (43)	20
$X183$	*abcadcbeed*	7	−0.0791 (29)	20
$X184$	*abcadcdeeb*	31	0.1973 (134)	25
$X185$	*abcadcebed*	5	−0.1269 (16)	10
$X186$	*abcadcedeb*	23	1.1883 (21)	10
$X187$	*abcadceebd*	6	1.2699 (27)	20
$X188$	*abcadceedb*	24	1.7966 (36)	11
$X189$	*abcaddbeec*	17	−3.7500 (105)	20
$X190$	*abcaddceeb*	33	−2.4966 (217)	20

TABLE I (continued): VEGAS integration results of $X001$–$X389$ of the tenth-order Set V diagrams.

Diagram	Vertex repr.	No. of subtr. terms	Value (Error) including n_F	No. of iterations with 10^9 sampling points per iteration
$X191$	*abcaddebec*	13	0.1892 (62)	11
$X192$	*abcaddeceb*	25	2.3868 (91)	24
$X193$	*abcaddeebc*	15	−4.2570 (84)	19
$X194$	*abcaddeecb*	27	−0.6785 (102)	25
$X195$	*abcadebcde*	2	−1.0708 (19)	10
$X196$	*abcadebced*	2	−2.0432 (20)	6
$X197$	*abcadebdce*	2	−0.3848 (8)	2
$X198$	*abcadebdec*	5	−2.3533 (26)	2
$X199$	*abcadebecd*	5	1.0636 (26)	2
$X200$	*abcadebedc*	11	0.0266 (26)	4
$X201$	*abcadecbde*	2	−0.4897 (18)	6
$X202$	*abcadecbed*	2	1.9313 (17)	6
$X203$	*abcadecdbe*	2	0.9061 (10)	4
$X204$	*abcadecdeb*	11	−1.9485 (26)	2
$X205$	*abcadecebd*	5	−0.9039 (13)	10
$X206$	*abcadecedb*	23	1.6836 (23)	10
$X207$	*abcadedbce*	5	0.2908 (23)	2
$X208$	*abcadedbec*	11	0.5283 (28)	2
$X209$	*abcadedcbe*	5	0.1496 (19)	2
$X210$	*abcadedceb*	23	0.7803 (19)	10
$X211$	*abcadedebc*	23	5.1339 (90)	12
$X212$	*abcadedecb*	41	−0.4617 (138)	25
$X213$	*abcadeebcd*	6	−2.4516 (29)	20
$X214$	*abcadeebdc*	12	0.6801 (39)	20
$X215$	*abcadeecbd*	6	0.0724 (24)	20
$X216$	*abcadeecdb*	24	−1.3029 (42)	12
$X217$	*abcadeedbc*	18	−2.2261 (71)	15
$X218$	*abcadeedcb*	30	−1.6396 (84)	25
$X219^{dd}$	*abcbaddeec*	39	1.3579 (311)	5
$X220$	*abcbadedec*	59	−2.5734 (222)	27
$X221$	*abcbadeecd*	35	0.6650 (161)	20
$X222$	*abcbadeedc*	51	0.8293 (178)	20
$X223^{dd}$	*abcbcdeeda*	116	17.5168 (349)	128
$X224$	*abcbdadeec*	31	2.4729 (110)	20
$X225$	*abcbdaedec*	23	0.3434 (39)	10
$X226$	*abcbdaeecd*	13	1.0443 (58)	11
$X227$	*abcbdaeedc*	25	0.5835 (97)	21
$X228$	*abcbdceeda*	75	−6.8113 (333)	52
$X229^{dd}$	*abcbddaeec*	35	−1.9843 (323)	11
$X230^{dd}$	*abcbddeeca*	71	15.6844 (350)	115

TABLE I (continued): VEGAS integration results of $X001$–$X389$ of the tenth-order Set V diagrams.

Diagram	Vertex repr.	No. of subtr. terms	Value (Error) including n_F	No. of iterations with 10^9 sampling points per iteration
$X231$	*abcbdeadec*	11	−0.7737 (28)	10
$X232$	*abcbdeaedc*	23	0.4608 (38)	10
$X233$	*abcbdecdea*	31	8.6698 (116)	25
$X234$	*abcbdeceda*	63	−2.5793 (179)	21
$X235$	*abcbdedaec*	23	0.7486 (35)	10
$X236$	*abcbdedcea*	63	2.0560 (180)	20
$X237$	*abcbdedeca*	113	−12.9913 (363)	154
$X238$	*abcbdeeadc*	25	1.2747 (45)	21
$X239$	*abcbdeecda*	69	−2.8075 (345)	49
$X240$	*abcbdeedca*	93	10.9428 (298)	55
$X241^{dd}$	*abccaddeeb*	43	13.8142 (357)	134
$X242$	*abccadedeb*	68	−10.4867 (377)	183
$X243^{dd}$	*abccadeedb*	57	3.8891 (336)	44
$X244^{dd}$	*abccdadeeb*	35	−3.3041 (334)	10
$X245$	*abccdaedeb*	27	0.0658 (83)	12
$X246$	*abccdaeedb*	29	−0.3959 (174)	20
$X247^{dd}$	*abccddaeeb*	39	15.9539 (344)	43
$X248^{dd}$	*abccddeaeb*	31	−1.9165 (278)	2
$X249$	*abccdeadeb*	13	4.0116 (46)	20
$X250$	*abccdeaedb*	27	−1.0558 (68)	24
$X251$	*abccdedaeb*	27	−1.3906 (76)	12
$X252^{dd}$	*abccdedeab*	56	−10.9091 (343)	31
$X253^{dd}$	*abccdedeba*	113	17.8437 (352)	221
$X254$	*abccdeeadb*	29	2.2265 (175)	20
$X255^{dd}$	*abccdeedab*	43	8.1598 (340)	6
$X256^{dd}$	*abccdeedba*	93	−14.0405 (342)	81
$X257$	*abcdabceed*	7	5.7475 (51)	11
$X258$	*abcdabdeec*	7	−0.5254 (39)	20
$X259$	*abcdabeced*	5	0.0053 (27)	10
$X260$	*abcdabedec*	5	−0.3958 (20)	2
$X261$	*abcdabeecd*	6	6.4046 (30)	20
$X262$	*abcdabeedc*	6	−2.2854 (24)	20
$X263$	*abcdacbeed*	7	−2.8330 (35)	20
$X264$	*abcdacdeeb*	15	4.8826 (64)	12
$X265$	*abcdacebed*	5	−0.6756 (20)	2
$X266$	*abcdacedeb*	11	0.1206 (23)	10
$X267$	*abcdaceebd*	6	−0.6608 (19)	20
$X268$	*abcdaceedb*	12	0.1185 (31)	20
$X269$	*abcdadbeec*	15	−0.7190 (56)	12
$X270$	*abcdadceeb*	31	−1.6881 (97)	25

TABLE I (continued): VEGAS integration results of $X001$–$X389$ of the tenth-order Set V diagrams.

Diagram	Vertex repr.	No. of subtr. terms	Value (Error) including n_F	No. of iterations with 10^9 sampling points per iteration
$X271$	*abcdadebec*	11	0.2492 (23)	10
$X272$	*abcdadeceb*	23	−0.7285 (32)	10
$X273$	*abcdadeebc*	13	−2.0474 (45)	11
$X274$	*abcdadeecb*	25	0.8675 (72)	24
$X275$	*abcdaebced*	2	−0.7496 (12)	10
$X276$	*abcdaebdce*	2	−0.5547 (10)	4
$X277$	*abcdaebdec*	2	2.7936 (10)	4
$X278$	*abcdaebecd*	5	−0.1577 (23)	10
$X279$	*abcdaebedc*	5	0.8399 (15)	2
$X280$	*abcdaecbed*	2	−1.0127 (8)	10
$X281$	*abcdaecdeb*	5	−1.3732 (25)	2
$X282$	*abcdaecebd*	5	0.4907 (18)	2
$X283$	*abcdaecedb*	11	−0.0427 (23)	2
$X284$	*abcdaedbec*	2	−0.2670 (9)	2
$X285$	*abcdaedceb*	5	0.0271 (16)	2
$X286$	*abcdaedebc*	11	0.8014 (21)	2
$X287$	*abcdaedecb*	23	0.2013 (19)	10
$X288$	*abcdaeebcd*	6	4.2112 (28)	20
$X289$	*abcdaeebdc*	6	−1.5651 (19)	20
$X290$	*abcdaeecbd*	6	−3.7763 (23)	20
$X291$	*abcdaeecdb*	12	1.5957 (32)	20
$X292$	*abcdaeedbc*	12	0.9114 (36)	20
$X293$	*abcdaeedcb*	24	−1.2653 (41)	11
$X294$	*abcdbaceed*	7	−3.3891 (25)	20
$X295$	*abcdbadeec*	7	1.7883 (26)	20
$X296$	*abcdbaeced*	5	0.5511 (13)	10
$X297$	*abcdbaedec*	5	−0.4696 (16)	10
$X298$	*abcdbaeecd*	6	−1.9142 (28)	20
$X299$	*abcdbaeedc*	6	−0.2907 (22)	20
$X300$	*abcdbceeda*	29	−9.4327 (194)	28
$X301$	*abcdbdaeec*	31	−1.3351 (81)	22
$X302$	*abcdbdeeca*	59	−1.8294 (223)	30
$X303$	*abcdbeadec*	2	0.3341 (7)	2
$X304$	*abcdbeaecd*	5	−0.3397 (16)	10
$X305$	*abcdbeaedc*	5	0.4715 (14)	2
$X306$	*abcdbeceda*	23	0.1228 (55)	20
$X307$	*abcdbedeca*	47	−0.3071 (59)	21
$X308$	*abcdbeeadc*	6	1.8122 (22)	20
$X309$	*abcdbeecda*	26	−4.2448 (173)	20
$X310$	*abcdbeedca*	50	0.2490 (191)	21

TABLE I (continued): VEGAS integration results of $X001$–$X389$ of the tenth-order Set V diagrams.

Diagram	Vertex repr.	No. of subtr. terms	Value (Error) including n_F	No. of iterations with 10^9 sampling points per iteration
$X311$	*abcdcabeed*	15	−0.5291 (58)	12
$X312$	*abcdcadeeb*	31	−1.2454 (139)	14
$X313$	*abcdcaebed*	11	0.9660 (38)	4
$X314$	*abcdcaedeb*	23	0.8266 (29)	10
$X315$	*abcdcaeebd*	13	−1.3728 (43)	20
$X316$	*abcdcaeedb*	25	0.0094 (39)	12
$X317$	*abcdcbeeda*	59	1.4535 (221)	23
$X318^{dd}$	*abcdcdaeeb*	62	−8.7568 (343)	59
$X319$	*abcdcdeaeb*	47	0.6801 (179)	25
$X320$	*abcdceadeb*	11	0.5627 (17)	10
$X321$	*abcdceaedb*	23	−0.9005 (26)	10
$X322$	*abcdcedaeb*	23	0.9338 (23)	2
$X323$	*abcdceeadb*	25	−0.0053 (40)	12
$X324$	*abcdceedab*	53	−8.8058 (243)	23
$X325$	*abcdceedba*	107	11.5958 (343)	51
$X326$	*abcddabeec*	17	−9.0047 (145)	24
$X327$	*abcddaceeb*	33	1.5517 (229)	29
$X328$	*abcddaebec*	13	−0.2781 (42)	20
$X329$	*abcddaeceb*	25	−0.9627 (67)	11
$X330$	*abcddaeebc*	15	−4.9591 (88)	14
$X331$	*abcddaeecb*	27	4.7241 (127)	25
$X332$	*abcddbaeec*	33	3.0539 (161)	25
$X333^{dd}$	*abcddbeeca*	65	6.8088 (341)	49
$X334^{dd}$	*abcddcaeeb*	47	5.1727 (340)	23
$X335$	*abcddceaeb*	37	−2.0294 (132)	25
$X336$	*abcddeabec*	6	−0.7685 (20)	20
$X337$	*abcddeaceb*	12	−1.2039 (32)	20
$X338$	*abcddeaebc*	13	−1.8505 (38)	20
$X339$	*abcddeaecb*	25	0.4111 (40)	12
$X340$	*abcddebeca*	53	−2.1543 (202)	25
$X341$	*abcddecaeb*	24	1.7815 (33)	20
$X342^{dd}$	*abcddeeacb*	27	2.6063 (125)	0
$X343$	*abcdeabced*	2	3.8873 (30)	6
$X344$	*abcdeabdce*	2	3.4223 (18)	6
$X345$	*abcdeabdec*	2	−1.0075 (18)	4
$X346$	*abcdeabecd*	2	0.2864 (20)	6
$X347$	*abcdeabedc*	2	−2.6846 (21)	6
$X348$	*abcdeacbed*	2	−0.4899 (15)	4
$X349$	*abcdeacdeb*	5	2.0800 (36)	2
$X350$	*abcdeacebd*	2	1.4643 (11)	4

TABLE I (continued): VEGAS integration results of $X001$–$X389$ of the tenth-order Set V diagrams.

Diagram	Vertex repr.	No. of subtr. terms	Value (Error) including n_F	No. of iterations with 10^9 sampling points per iteration
$X351$	*abcdeacedb*	5	0.2554 (20)	2
$X352$	*abcdeadbec*	2	−0.1260 (8)	2
$X353$	*abcdeadceb*	5	0.1950 (16)	2
$X354$	*abcdeadebc*	5	−2.0503 (20)	2
$X355$	*abcdeadecb*	11	−1.0738 (25)	2
$X356$	*abcdeaebcd*	5	2.0684 (24)	10
$X357$	*abcdeaebdc*	5	0.3746 (16)	2
$X358$	*abcdeaecbd*	5	0.0463 (16)	2
$X359$	*abcdeaecdb*	11	−0.1396 (17)	10
$X360$	*abcdeaedbc*	11	−0.4604 (37)	2
$X361$	*abcdeaedcb*	23	2.5600 (26)	10
$X362$	*abcdebadec*	2	−0.5714 (12)	4
$X363$	*abcdebaecd*	2	−2.3442 (19)	4
$X364$	*abcdebaedc*	2	2.3957 (18)	4
$X365$	*abcdebceda*	11	0.4177 (30)	20
$X366$	*abcdebdeca*	23	5.6759 (43)	20
$X367$	*abcdebeadc*	5	−0.7176 (12)	10
$X368$	*abcdebecda*	23	−0.3404 (45)	20
$X369$	*abcdebedca*	47	−3.3812 (59)	21
$X370$	*abcdecadeb*	5	−1.4763 (12)	10
$X371$	*abcdecaedb*	5	0.0045 (10)	2
$X372$	*abcdecdaeb*	11	−1.2900 (33)	2
$X373$	*abcdeceadb*	23	0.5851 (24)	2
$X374$	*abcdecedab*	47	0.9188 (266)	18
$X375$	*abcdecedba*	89	1.0991 (163)	25
$X376$	*abcdedabec*	5	1.0484 (16)	2
$X377$	*abcdedaceb*	11	0.4264 (27)	2
$X378$	*abcdedaebc*	11	1.3196 (21)	2
$X379$	*abcdedaecb*	23	−0.3201 (17)	10
$X380$	*abcdedbeca*	47	−1.0268 (48)	21
$X381$	*abcdedcaeb*	23	1.0861 (29)	2
$X382$	*abcdedeacb*	41	−1.7712 (80)	21
$X383$	*abcdeeabdc*	6	−4.8034 (22)	20
$X384$	*abcdeeacdb*	12	1.9266 (31)	20
$X385$	*abcdeeadbc*	12	−0.7427 (19)	20
$X386$	*abcdeeadcb*	24	0.6887 (38)	11
$X387$	*abcdeebdca*	50	1.9508 (152)	21
$X388$	*abcdeecadb*	24	−0.4349 (40)	20
$X389$	*abcdeedacb*	30	−0.0433 (68)	25

TABLE II: Residual renormalization constants used to calculate $a_e^{(10)}$[Set V]. Notations are those of Eq. (35).

Integral	Value (Error)	Integral	Value (Error)
ΔM_{10}	3.468 (336)	ΔL_{4^*}	−0.459 051 (62)
ΔM_8	1.738 12 (85)	ΔL_{2^*}	−0.75
ΔM_6	0.425 8135 (30)	Δdm_6	−2.340 815 (55)
ΔM_4	0.030 833 612 $\cdots$	Δdm_4	1.906 3609 (90)
M_2	0.5	Δdm_{2^*}	−0.75
ΔLB_8	2.0504 (86)		
ΔLB_6	0.100 801 (43)		
ΔLB_4	0.027 9171 (61)		
ΔLB_2	0.75		

Acknowledgments

This work is supported in part by the JSPS Grant-in-Aid for Scientific Research (C)20540261 and (C)23540331. T. K.'s work is supported in part by the U. S. National Science Foundation under Grant No. NSF-PHY-0757868. T. K. thanks RIKEN for the hospitality extended to him while a part of this work was carried out. Numerical calculations are conducted on the RIKEN Super Combined Cluster System (RSCC) and the RIKEN Integrated Cluster of Clusters (RICC) supercomputing systems.

Appendix A: *K*-operation, *R*-subtraction, and (modified) *I*-operation on the diagram X253

This Appendix is devoted to the discussion of the diagram X253 shown in Fig. 2. We describe in some detail the relation between the standard on-shell renormalization and the renormalization method adopted by GENCODE*N* based on the *K*-operation, *R*-subtraction, and *I*-subtraction, choosing X253 as an example. Actually, X253 and another diagram X256 are not entirely typical in the sense that they require a slight modification of one of the *I*-subtraction operations encoded in GENCODE*N*. The reason why this modification is required and its resolution will be discussed in detail.

In this Appendix, we adopt the following notations. Internal lepton lines are numbered *1, 2, 3, 4, 5, 6, 7, 8, 9* from left to right, and internal photon lines are numbered *a, b, c, d, e* as shown in Fig. 2. Subdiagrams are represented by the set of indices enclosed in braces.

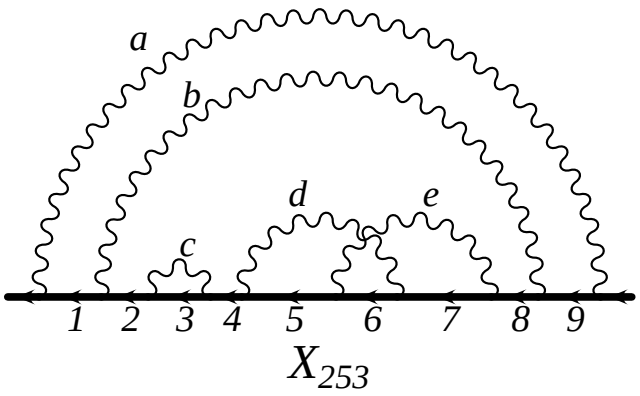

FIG. 2: Diagram X253.

The subtraction operators are labelled by the indices of lepton lines of the subdiagrams: For example, the K-operation applied to the self-energy subdiagram $\{3;\ c\}$ is denoted as $\mathbb{K}_3$. The R-subtraction applied to the self-energy-like subdiagram $\{5\ 6\ 7;\ d\ e\}$ is denoted as $\mathbb{R}_{567}$. The I-subtraction applied to the self-energy-like subdiagram $\{2\ 3\ 4\ 5\ 6\ 7\ 8;\ b\ c\ d\ e\}$ is denoted as $\mathbb{I}_{19}$ using the indices of the residual diagram $\{1\ 9;\ a\}$ which is obtained by reducing the subdiagram to a point. For the nested I-subtractions applied to subdiagrams $\mathcal{S}_1$ and $\mathcal{S}_2$ where $\mathcal{S}_1 \supset \mathcal{S}_2$, the operators are labelled by the indices in the reduced subdiagrams $\mathcal{G}/\mathcal{S}_1$ and $\mathcal{S}_1/\mathcal{S}_2$, respectively. Other cases are denoted in a similar manner accordingly.

1. Standard renormalization

The diagram X253 has UV divergences arising from the following subdiagrams: $\{3;\ c\}$, $\{5\ 6\ 7;\ d\ e\}$, $\{5\ 6;\ d\}$, $\{6\ 7;\ e\}$, $\{2\ 3\ 4\ 5\ 6\ 7\ 8;\ b\ c\ d\ e\}$. Recalling that Fig. 2 actually represents the sum of nine vertex diagrams containing various subdiagrams of vertex type

and self-energy type, we can write the standard renormalization of X253 as follows:

$$
\begin{aligned}
a_{\mathrm{X253}} &= M_{\mathrm{X253}} + M_{30}\ (-2\ L_2) + M_{42}\ (-B_2) + M_{42(2^*)}\ (-dm_2) \\
&+ M_{6b}\ (-B_{4a} + 4\ L_2\ B_2) + M_{6b(2^*)}\ (-dm_{4a} + 4\ L_2\ dm_2) \\
&+ M_{4b}\ \{B_{4a}\ B_2 - 2\ L_2\ (B_2)^2\} + M_{4b(2^*)}\ \{dm_{4a} B_2 + dm_2\ (B_{4a} - 4\ L_2\ B_2)\} \\
&+ M_{4b(2^{**})}\ dm_2\ (dm_{4a} - 2\ L_2\ dm_2) \\
&+ M_2\ [-B_{16} + 2\ B_{6a}\ L_2 + B_{6c}\ B_2 + B_{4a}\ \{B_{4b} - (B_2)^2\} \\
&\quad -4\ B_{4b}\ L_2\ B_2 + 2\ L_2\ (B_2)^3 + dm_{4a}\ (B_{4b(1^*)} - B_2\ B_{2^*})] \\
&+ M_2\ dm_2\ \{B_{6c(1^*)} - 4\ L_2\ B_{4b(1^*)} - B_{2^{**}}\ dm_{4a} - B_{2^*}\ B_{4a} \\
&\quad +2\ L_2\ (dm_2\ B_{2^{**}} + 2\ B_2\ B_{2^*})\} \\
&+ M_{2^*}\ dm_2\ [dm_{6c(1^*)} - B_{4a}(dm_{2^*} + B_2) - dm_{2^{**}}\ dm_{4a} - 4\ L_2\ dm_{4b(1^*)} \\
&\quad +2\ L_2\{(B_2)^2 + 2\ B_2\ dm_{2^*} + dm_2\ dm_{2^{**}}\}] \\
&+ M_{2^*}\ \{-dm_{16} + 2\ dm_{6a}\ L_2 + dm_{6c}\ B_2 \\
&\quad +dm_{4a}\ (dm_{4b(1^*)} - B_2\ dm_{2^*}) + dm_{4b}\ (B_{4a} - 4\ L_2\ B_2)\}
\end{aligned}
\tag{A1}
$$

where the suffixes 16, 30, and 42 are those identifying eighth-order subdiagrams [11]. Suffixes $6a$, $6b$, $6c$ refer to the sixth-order subdiagrams, and $4a$,$4b$ refer to the fourth-order subdiagrams. Symbols (i^*) in the suffixes refer to the diagrams derived by insertion of a two-point vertex in the lepton line i. (i^{**}) corresponds to two insertions of vertices. For second-order diagrams, the parenthesis and the index i are omitted for simplicity. See Ref. [11] for the explanation of other notations. All terms on the right-hand side of (A1) contain UV divergent parts. Thus some regularization is assumed.

2. Separation of UV divergences by K-operation

The first step is to separate UV-divergent parts of all terms on the right-hand side of (A1) from their UV-finite parts. We carry out this separation by means of K-operation starting with M_{X253}.

M_{X253} has no overall UV divergence. It has only UV divergences from some subdiagrams. The UV-divergence-free part $M^{\mathrm{R}}_{\mathrm{X253}}$ of M_{X253} is defined by the K-operations as

$$
M^{R}_{\mathrm{X253}} = \sum_{f \in \mathfrak{F}(\mathcal{G})} \left[\prod_{\mathcal{S}_i \in f} (-\mathbb{K}_{\mathcal{S}_i}) \right] M_{\mathrm{X253}}, \tag{A2}
$$

where the sum is over 24 forests constructed from the five subdiagrams including the empty forest. Note that the forest corresponding to $\mathbb{K}_{56}\mathbb{K}_{67}$ is absent since the subdiagrams $\{5\ 6;\ d\}$ and $\{6\ 7;\ e\}$ overlap each other.

Carrying out the K-operations explicitly (see Sec. III D), and rewriting the result as an expression of $M_{\rm X253}$, we obtain

$$\begin{aligned}
M_{\rm X253} \;=\;& M^{\rm R}_{\rm X253} + M_{30}\ (2\ L_2^{\rm UV}) + M_{42}\ (B_2^{\rm UV}) + M_{42(2^*)}\ (dm_2^{\rm UV}) \\
&+\ M_{6b}\ (B_{4a}^{\rm UV} - 4\ L_2^{\rm UV}\ B_2^{\rm UV}) + M_{6b(2^*)}\ (dm_{4a}^{\rm UV} - 4\ L_2^{\rm UV}\ dm_2^{\rm UV}) \\
&+\ M_{4b}\ \{-B_{4a}^{\rm UV}\ B_2^{\rm UV} + 2\ L_2^{\rm UV}\ (B_2^{\rm UV})^2\} \\
&+\ M_{4b(2^*)}\ \{-dm_{4a}^{\rm UV}\ B_2^{\rm UV} + dm_2^{\rm UV}\ (-B_{4a}^{\rm UV} + 4\ B_2^{\rm UV}\ L_2^{\rm UV})\} \\
&+\ M_{4b(2^{**})}\ dm_2^{\rm UV}\ (-dm_{4a}^{\rm UV} + 2\ L_2^{\rm UV}\ dm_2^{\rm UV}) \\
&+\ M_2\ [B_{16}^{\rm UV} - 2\ B_{6a}^{\rm UV}\ L_2^{\rm UV} - B_{6c(1')}^{\rm UV}\ B_2^{\rm UV} + B_{4a}^{\rm UV}\ (-B_{4b(1')}^{\rm UV} + B_2^{\rm UV}\ B_{2''}^{\rm UV}) \\
&\quad +4\ B_{4b(1')}^{\rm UV}\ L_2^{\rm UV}\ B_2^{\rm UV} - 2\ L_2^{\rm UV}\ (B_2^{\rm UV})^2\ B_{2''}^{\rm UV}] \\
&+\ M_{2^*}[dm_2^{\rm UV}\{-\ dm_{6c(1^*)}^{\rm UV} + B_{4a}^{\rm UV}\ dm_{2^{*\prime}}^{\rm UV} + 4\ L_2^{\rm UV}\ dm_{4b(1^*)}^{\rm UV} - 4\ L_2^{\rm UV}\ B_2^{\rm UV}\ dm_{2^{*\prime}}^{\rm UV}\} \\
&\quad +dm_{2''}^{\rm UV}\{B_{4a}^{\rm UV}\ B_2^{\rm UV} - 2\ L_2^{\rm UV}\ (B_2^{\rm UV})^2\}] \\
&+\ M_{2^*}\ \{dm_{16}^{\rm UV} - 2\ dm_{6a}^{\rm UV}\ L_2^{\rm UV} - dm_{6c(1')}^{\rm UV}\ B_2^{\rm UV} \\
&\quad +dm_{4a}^{\rm UV}\ (-dm_{4b(1^*)}^{\rm UV} + B_2^{\rm UV}\ dm_{2^{*\prime}}^{\rm UV}) + dm_{4b(1')}^{\rm UV}(-B_{4a}^{\rm UV} + 4\ L_2^{\rm UV}\ B_2^{\rm UV})\}. \qquad \text{(A3)}
\end{aligned}$$

Here, quantities with primes (i') in the suffixes denote the derivative amplitudes related to those without primes, where the index i refers to the lepton line to insert derivative. For the second order case the index is omitted for simplicity. See Ref. [48] for further explanations.

The next step is to substitute (A3) in (A1). Since the result of substitution contains eighth-order terms M_{30}, M_{42}, etc., which are UV-divergent, we must substitute them by the K-operation results of M_{30}, M_{42}, etc., listed below:

$$\begin{aligned}
M_{30} \;=\;& M^{\rm R}_{30} + 2dm_2^{\rm UV} M_{6b(2^*)} + 2B_2^{\rm UV} M_{6b} + dm_{6a}^{\rm UV} M_{2^*} + B_{6a}^{\rm UV} M_2 \\
&-\ dm_2^{\rm UV}(dm_2^{\rm UV} M_{4b(2^{**})} + B_2^{\rm UV} M_{4b(2^*)}) - B_2^{\rm UV}(dm_2^{\rm UV} M_{4b(2^*)} + B_2^{\rm UV} M_{4b}) \\
&-\ 2dm_2^{\rm UV} dm_{4b(1^*)}^{\rm UV} M_{2^*} - 2B_2^{\rm UV}(dm_{4b(1')}^{\rm UV} M_{2^*} + B_{4b(1')}^{\rm UV} M_2) \\
&+\ 2dm_2^{\rm UV} B_2^{\rm UV} dm_{2^{*\prime}}^{\rm UV} M_{2^*} + (B_2^{\rm UV})^2(dm_{2''}^{\rm UV} M_{2^*} + B_{2''}^{\rm UV} M_2), \qquad \text{(A4)}
\end{aligned}$$

$$
\begin{aligned}
M_{42} &= M_{42}^{\rm R} + 2L_2^{\rm UV} M_{6b} + dm_{4a}^{\rm UV} M_{4b(2^*)} + B_{4a}^{\rm UV} M_{4b} + dm_{6c}^{\rm UV} M_{2^*} + B_{6c}^{\rm UV} M_2 \\
&- 2L_2^{\rm UV}(dm_2^{\rm UV} M_{4b(2^*)} + B_2^{\rm UV} M_{4b}) - 2L_2^{\rm UV}(dm_{4b}^{\rm UV} M_{2^*} + B_{4b}^{\rm UV} M_2) \\
&- dm_{4a}^{\rm UV} dm_{2^*}^{\rm UV} M_{2^*} - B_{4a}^{\rm UV}(dm_{2'}^{\rm UV} M_{2^*} + B_{2'}^{\rm UV} M_2) \\
&+ 2L_2^{\rm UV} dm_2^{\rm UV} dm_{2^*}^{\rm UV} M_{2^*} + 2L_2^{\rm UV} B_2^{\rm UV}(dm_{2'}^{\rm UV} M_{2^*} + B_{2'}^{\rm UV} M_2), \qquad \text{(A5)}
\end{aligned}
$$

$$
\begin{aligned}
B_{16} &= B_{16}^{\rm UV} + B_{16}^{\rm R} + 2L_2^{\rm UV}\widetilde{B_{6a}} + dm_2^{\rm UV} B_{6c(1^*)} + B_2^{\rm UV}\widetilde{B_{6c(1')}} \\
&+ (dm_{4a}^{\rm UV} - 4dm_2^{\rm UV} L_2^{\rm UV}) B_{4b(1^*)} + (B_{4a}^{\rm UV} - 4L_2^{\rm UV} B_2^{\rm UV})\widetilde{B_{4b(1')}} \\
&+ (-B_2^{\rm UV} dm_{4a}^{\rm UV} - dm_2^{\rm UV} B_{4a}^{\rm UV} + 4dm_2^{\rm UV} L_2^{\rm UV} B_2^{\rm UV}) B_{2^{*\prime}} \\
&- dm_2^{\rm UV}(dm_{4a}^{\rm UV} - 2L_2^{\rm UV} dm_2^{\rm UV}) B_{2^{**}} - B_2^{\rm UV}(B_{4a}^{\rm UV} - 2L_2^{\rm UV} B_2^{\rm UV})\widetilde{B_{2''}}, \qquad \text{(A6)}
\end{aligned}
$$

$$
\begin{aligned}
dm_{16} &= dm_{16}^{\rm UV} + dm_{16}^{\rm R} + 2L_2^{\rm UV}\widetilde{dm_{6a}} + dm_2^{\rm UV}\widetilde{dm_{6c(1^*)}} + B_2^{\rm UV}\widetilde{dm_{6c(1')}} \\
&+ (dm_{4a}^{\rm UV} - 4dm_2^{\rm UV} L_2^{\rm UV})\widetilde{dm_{4b(1^*)}} + (B_{4a}^{\rm UV} - 4L_2^{\rm UV} B_2^{\rm UV})\widetilde{dm_{4b(1')}} \\
&+ (-B_2^{\rm UV} dm_{4a}^{\rm UV} - dm_2^{\rm UV} B_{4a}^{\rm UV} + 4dm_2^{\rm UV} L_2^{\rm UV} B_2^{\rm UV})\widetilde{dm_{2^{*\prime}}} \\
&- dm_2^{\rm UV}(dm_{4a}^{\rm UV} - 2L_2^{\rm UV} dm_2^{\rm UV}) dm_{2^{**}} - B_2^{\rm UV}(B_{4a}^{\rm UV} - 2L_2^{\rm UV} B_2^{\rm UV})\widetilde{dm_{2''}}, \qquad \text{(A7)}
\end{aligned}
$$

and so on, where $\widetilde{B_{6a}} \equiv B_{6a} - B_{6a}^{\rm UV}$, etc. Note that M_{30} and M_{42} have UV divergences coming from subdiagrams but no overall UV divergences whereas renormalization constants B_{16} and dm_{16} have overall UV divergences.

Since the result of substitution of (A7) still contains M_{6a}, etc., which have UV-divergent subdiagrams, it is necessary to separate their UV-divergent parts using

$$
\begin{aligned}
M_{6b} &= M_{6b}^{\rm R} + dm_2^{\rm UV} M_{4b(2^*)} + B_2^{\rm UV} M_{4b} + (dm_{4b}^{\rm UV} - dm_2^{\rm UV} dm_{2^*}^{\rm UV}) M_{2^*} \\
&+ B_{4b}^{\rm UV} M_2 - B_2^{\rm UV}(dm_{2'}^{\rm UV} M_{2^*} + B_{2'}^{\rm UV} M_2), \\
M_{6b(2^*)} &= M_{6b(2^*)}^{\rm R} + dm_2^{\rm UV} M_{4b(2^{**})} + B_2^{\rm UV} M_{4b(2^*)} + dm_{4b(1^*)}^{\rm UV} M_{2^*} - dm_{2^{*\prime}}^{\rm UV} B_2^{\rm UV} M_{2^*}, \qquad \text{(A8)}
\end{aligned}
$$

$$
\begin{aligned}
B_{6a} &= B_{6a}^{\rm UV} + B_{6a}^{\rm R} + 2(dm_2^{\rm UV} B_{4b(1^*)} + B_2^{\rm UV}\widetilde{B_{4b(1')}}) - dm_2^{\rm UV}(dm_2^{\rm UV} B_{2^{**}} + B_2^{\rm UV} B_{2^*}) \\
&- B_2^{\rm UV}(dm_2^{\rm UV} B_{2^*} + B_2^{\rm UV}\widetilde{B_{2''}}), \\
B_{6c} &= B_{6c}^{\rm UV} + B_{6c}^{\rm R} + 2L_2^{\rm UV}\widetilde{B_{4b}} + dm_{4a}^{\rm UV} B_{2^*} + B_{4a}^{\rm UV}\widetilde{B_{2'}} \\
&- 2L_2^{\rm UV}(dm_2^{\rm UV} B_{2^*} + B_2^{\rm UV}\widetilde{B_{2'}}), \qquad \text{(A9)}
\end{aligned}
$$

$$\begin{aligned}
dm_{6a} &= dm_{6a}^{\rm UV} + dm_{6a}^{\rm R} + 2(dm_2^{\rm UV}\widetilde{dm_{4b(1^*)}} + B_2^{\rm UV}\widetilde{dm_{4b(1')}}) - dm_2^{\rm UV}(dm_2^{\rm UV} dm_{2^{**}} + B_2^{\rm UV}\widetilde{dm_{2^{*\prime}}}) \\
&- B_2^{\rm UV}(dm_2^{\rm UV}\widetilde{dm_{2^{*\prime}}} + B_2^{\rm UV}\widetilde{dm_{2''}}), \\
dm_{6c} &= dm_{6c}^{\rm UV} + dm_{6c}^{\rm R} + 2L_2^{\rm UV}\widetilde{dm_{4b}} + dm_{4a}^{\rm UV}\widetilde{dm_{2^*}} + B_{4a}^{\rm UV}\widetilde{dm_{2'}} \\
&- 2L_2^{\rm UV}(dm_2^{\rm UV}\widetilde{dm_{2^*}} + B_2^{\rm UV}\widetilde{dm_{2'}}),
\end{aligned} \tag{A10}$$

followed by

$$\begin{aligned}
M_{4b} &= M_{4b}^{\rm R} + dm_2^{\rm UV} M_{2^*} + B_2^{\rm UV} M_2, \\
M_{4b(2^*)} &= M_{4b(2^*)}^{\rm R} + dm_{2^*}^{\rm UV} M_{2^*}, \\
B_{4a} &= B_{4a}^{\rm UV} + B_{4a}^{\rm R} + 2L_2^{\rm UV} B_2^{\rm R}, \\
B_{4b} &= B_{4b}^{\rm UV} + B_{4b}^{\rm R} + dm_2^{\rm UV} B_{2^*} + B_2^{\rm UV} B_{2'}^{\rm R}, \\
B_{4b(1^*)} &= B_{4b(1^*)}^{\rm R} + dm_2^{\rm UV} B_{2^{**}} + B_2^{\rm UV} B_{2^*}, \\
dm_{4a} &= dm_{4a}^{\rm UV} + dm_{4a}^{\rm R}, \qquad \text{(A11)} \\
dm_{4b} &= dm_{4b}^{\rm UV} + dm_{4b}^{\rm R} + dm_2^{\rm UV} dm_{2^*}^{\rm R} + B_2^{\rm UV} dm_{2'}^{\rm R}, \\
dm_{4b(1^*)} &= dm_{4b(1^*)}^{\rm UV} + dm_{4b(1^*)}^{\rm R} + dm_2^{\rm UV} dm_{2^{**}} + B_2^{\rm UV}\widetilde{dm_{2^{*\prime}}}, \qquad \text{(A12)} \\
L_2 &= L_2^{\rm UV} + L_2^{\rm R}, \\
B_2 &= B_2^{\rm UV} + B_2^{\rm R}, \\
dm_{2^*} &= dm_{2^*}^{\rm UV} + dm_{2^*}^{\rm R}. \qquad \text{(A13)}
\end{aligned}$$

After all UV divergences are separated out by successive K-operations, we can at last express $a_{\rm X253}$ in terms of UV-finite quantities only:

$$\begin{aligned}
a_{\rm X253} &= M_{\rm X253}^{\rm R} + M_{30}^{\rm R}\ (-2\ L_2^{\rm R}) + M_{42}^{\rm R}\ (-B_2^{\rm R}) \\
&+ M_{6b}^{\rm R}\ (-B_{4a}^{\rm R} + 4\ L_2^{\rm R}\ B_2^{\rm R}) + M_{6b(2^*)}^{\rm R}\ (-dm_{4a}^{\rm R}) \\
&+ M_{4b}^{\rm R}\ \{B_{4a}^{\rm R}\ B_2^{\rm R} - 2\ L_2^{\rm R}\ (B_2^{\rm R})^2\} + M_{4b(2^*)}^{\rm R}\ dm_{4a}^{\rm R}\ B_2^{\rm R} \\
&+ M_2\ [-B_{16}^{\rm R} + 2\ B_{6a}^{\rm R}\ L_2^{\rm R} + B_{6c}^{\rm R}\ B_2^{\rm R} + B_{4a}^{\rm R}\ \{B_{4b}^{\rm R} - (B_2^{\rm R})^2\} \\
&\quad -4\ B_{4b}^{\rm R}\ L_2^{\rm R}\ B_2^{\rm R} + 2\ L_2^{\rm R}\ (B_2^{\rm R})^3 + dm_{4a}^{\rm R}\ (B_{4b(1^*)}^{\rm R} - B_{2^*}\ B_2^{\rm R})] \\
&+ M_{2^*}\ \{-dm_{16}^{\rm R} + 2\ dm_{6a}^{\rm R}\ L_2^{\rm R} + dm_{6c}^{\rm R}\ B_2^{\rm R} \\
&\quad +dm_{4a}^{\rm R}\ (dm_{4b(1^*)}^{\rm R} - B_2^{\rm R}\ dm_{2^*}^{\rm R}) + dm_{4b}^{\rm R}\ (B_{4a}^{\rm R} - 4\ L_2^{\rm R}\ B_2^{\rm R})\}.
\end{aligned} \tag{A14}$$

Note that (A14) has exactly the same structure as (A1) but looks simpler because $dm_2^{\rm R} \equiv dm_2 - dm_2^{\rm UV} = 0$.

3. Separation of IR divergences by *R*-subtraction and *I*-subtraction

The integrands of $M^{\rm R}_{\rm X253}$, etc., are singular at vanishing momenta of virtual photons because of vanishing photon mass. When the integrands are integrated over all momenta, these singularities give rise to logarithmic IR divergences (if enhanced by vanishing denominators of two lepton propagators which are adjacent to the external lines) or linear IR divergences (if enhanced by three lepton propagators).

To prepare for the numerical integration it is necessary to separate the IR-divergent parts from the IR-finite parts, and integrate only the latter parts. Since the sum of all diagrams of Set V is gauge-invariant and finite, IR-divergent parts cancel out when summed over all diagrams of Set V.

As we have discussed in Ref. [23] and Sec. III E, the IR divergences in the amplitude $M^{\rm R}_{\rm X253}$ can be handled completely by looking at the self-energy-like subdiagram $\mathcal{S}$ of X253. They are $\mathcal{S}_1 = \{2\ 3\ 4\ 5\ 6\ 7\ 8;\ b\ c\ d\ e\}$, $\mathcal{S}_2 = \{5\ 6\ 7;\ d\ e\}$, and $\mathcal{S}_3 = \{3;\ c\}$. There are two subtraction schemes, *R*-subtraction to deal with the linear IR divergence, and *I*-subtraction to deal with the logarithmic IR divergence:

- *R*-subtraction annotates M and dm to the whole diagram $\mathcal{G}$ and some of the subdiagrams $\mathcal{S}$, respectively. Following the procedure built into GENCODE*N* *R*-subtraction $\mathbb{R}_{\mathcal{S}}$ is applied to the subdiagram $\mathcal{S}$. The reduced diagram $\mathcal{G}/\mathcal{S}$ gives rise to a magnetic moment amplitude of lower order.

- *I*-subtraction annotates I and M to the whole diagram $\mathcal{G}$ and some of the subdiagrams $\mathcal{S}$, respectively. Then *I*-subtraction $\mathbb{I}_{\mathcal{S}}$ is applied to the reduced diagram $\mathcal{G}/\mathcal{S}$ and the subdiagram $\mathcal{S}$ gives rise to a magnetic moment amplitude of lower order.

- In addition there are cases where *R*-subtraction and *I*-subtraction occur together.

The diagram X253 has 11 annotated forests. GENCODE*N* generates IR subtraction terms

as follows:

annotation	subtraction	expression
$\mathcal{G} \to M, \quad \mathcal{S}_1 \to dm$	$\mathbb{R}_{2-8}$	$dm^{\rm R}_{16} M_{2^*}$
$\mathcal{G} \to M, \quad \mathcal{S}_2 \to dm$	$\mathbb{R}_{567}$	$dm^{\rm R}_{4a} M^{\rm R}_{6b(2^*)}$
$\mathcal{G} \to M, \quad \mathcal{S}_1 \to dm, \quad \mathcal{S}_2 \to dm$	$\mathbb{R}_{2-8}\mathbb{R}_{567}$	$dm^{\rm R}_{4b(1^*)} dm^{\rm R}_{4a} M_{2^*}$
$\mathcal{G} \to I, \quad \mathcal{S}_1 \to M$	$\mathbb{I}_{19}$	$L^{\rm R}_2 M^{\rm R}_{16}$
$\mathcal{G} \to I, \quad \mathcal{S}_2 \to M$	$\mathbb{I}_{123489}$	$L^{\rm R}_{6b(2)} M^{\rm R}_{4a}$
$\mathcal{G} \to I, \quad \mathcal{S}_3 \to M$	$\mathbb{I}_{12456789}$	$L^{\rm R}_{42(2)} M_2$
$\mathcal{G} \to I, \quad \mathcal{S}_1 \to I, \quad \mathcal{S}_2 \to M$	$\mathbb{I}_{19}\mathbb{I}_{2348}$	$L^{\rm R}_2 L^{\rm R}_{4b1} M^{\rm R}_{4a}$
$\mathcal{G} \to I, \quad \mathcal{S}_1 \to I, \quad \mathcal{S}_3 \to M$	$\mathbb{I}_{19}\mathbb{I}_{245678}$	$L^{\rm R}_2 L^{\rm R}_{6c(1)} M_2$
$\mathcal{G} \to I, \quad \mathcal{S}_1 \to M, \quad \mathcal{S}_2 \to dm$	$\mathbb{I}_{19}\mathbb{R}_{567}$	$L^{\rm R}_2 dm^{\rm R}_{4a} M^{\rm R}_{4b(1^*)}$
$\mathcal{G} \to I, \quad \mathcal{S}_3 \to M, \quad \mathcal{S}_2 \to dm$	$\mathbb{I}_{12489}\mathbb{R}_{567}$	$L^{\rm R}_{4b2(2^*)} dm^{\rm R}_{4a} M_2$
$\mathcal{G} \to I, \quad \mathcal{S}_1 \to I, \quad \mathcal{S}_3 \to M, \quad \mathcal{S}_2 \to dm$	$\mathbb{I}_{19}\mathbb{I}_{248}\mathbb{R}_{567}$	$L^{\rm R}_2 L^{\rm R}_{2^*} dm^{\rm R}_{4a} M_2$

Here, $\mathbb{R}_{2-8}$ is an abbreviation of $\mathbb{R}_{2345678}$.

In the diagram $M^{\rm R}_{\rm X253}$ one of the linear IR divergences occurs when the momentum of the outermost photon *a* vanishes. The self-energy-like subdiagram {*2 3 4 5 6 7 8; b c d e*} behaves as a self-mass term, because the adjacent lepton propagators *1* and *9* are almost on-the-mass-shell in this limit. The reduced diagram {*1 9; a*} then gives rise to a magnetic moment M_{2^*}, which is linearly IR divergent because of a two-point vertex insertion.

In the *K*-operation, however, only the UV-divergent part of the mass renormalization term is subtracted. This is why (A14) contains the unsubtracted UV-finite parts of mass renormalization terms, such as $dm^{\rm R}_{16}$, which gives rise to a linearly IR divergent term proportional to M_{2^*} [2]. To remove this linear IR divergence we have only to complete the standard mass-renormalization by subtracting also the remaining part of mass-renormalization term. This is the procedure called *R*-subtraction. For instance the operation of $\mathbb{R}_{2-8}$ on $M^{\rm R}_{\rm X253}$, implemented on GENCODE*N*, yields

$$\mathbb{R}_{2-8} M^{\rm R}_{\rm X253} = M_{2^*} dm^{\rm R}_{16}, \tag{A15}$$

where $dm^{\rm R}_{16}$ is defined in (A7).

[2] The linear IR divergent terms in M_{2^*} exactly cancel out within M_{2^*} itself and the analytic value of $M_{2^*} = 1$ is finite. The cancellation, however, does not occur in numerical integration of our parametric integral formula M_{2^*} and it suffers from the linear IR divergence.

Once all linear IR divergences are removed by R-subtractions we are left with logarithmic IR divergences. When the self-energy-like subdiagram $\mathcal{S}$ behaves as a magnetic moment amplitude of lower order and can be mimicked by a point (vector) vertex, the *outer* residual diagram $\mathcal{R} = \mathcal{G}/\mathcal{S}$ behaves like a vertex diagram and its IR behavior is exactly the same as that of the vertex renormalization constant extracted from $\mathcal{R}$. We find several residual diagrams: $\{1\ 9;\ a\}$ for the residual diagram of $\mathcal{S}_1$, $\{1\ 2\ 3\ 4\ 8\ 9;\ a\ b\ c\}$ for $\mathcal{S}_2$, $\{1\ 2\ 4\ 5\ 6\ 7\ 8\ 9;\ a\ b\ d\ e\}$ for $\mathcal{S}_3$, as well as the combinations of $\{1\ 9;\ a\}$ with the other two.

For $\mathcal{R} = \{1\ 9;\ a\}$, the IR divergence can be extracted by the I-subtraction

$$\mathbb{I}_{19} M^{\mathrm{R}}_{\mathrm{X253}} = L^{\mathrm{R}}_2 M^{\mathrm{R}}_{16}, \tag{A16}$$

where L^{R}_2, which is logarithmically IR divergent, is the UV-finite part of the second-order vertex renormalization constant L_2, and M^{R}_{16} is the UV-divergence-free part of the eighth-order magnetic moment M_{16}.

In addition the I-subtraction works on the linearly IR-divergent terms such as $\mathbb{R}_{567} M^{\mathrm{R}}_{\mathrm{X253}}$. The IR divergence subtraction scheme in GENCODEN will give rise to

$$\mathbb{I}_{19}\mathbb{R}_{567} M^{\mathrm{R}}_{\mathrm{X253}} = dm^{\mathrm{R}}_{4a} L^{\mathrm{R}}_2 M^{\mathrm{R}}_{4b(1^*)}, \tag{A17}$$

$$\mathbb{I}_{12489}\mathbb{R}_{567} M^{\mathrm{R}}_{\mathrm{X253}} = dm^{\mathrm{R}}_{4a} L^{\mathrm{R}}_{4b2(2^*)} M_2, \tag{A18}$$

$$\mathbb{I}_{19}\mathbb{I}_{248}\mathbb{R}_{567} M^{\mathrm{R}}_{\mathrm{X253}} = dm^{\mathrm{R}}_{4a} L^{\mathrm{R}}_2 L^{\mathrm{R}}_{2^*} M_2. \tag{A19}$$

It is easy to check that (A17) gives a correct IR-divergent term as expected. It turns out, however, that the prescription encoded in GENCODEN for the construction of the subtraction terms (A18) and (A19) has some discrepancy from the formulation that stems from the choice in the separation of the finite and divergent parts of the term L^*, and it actually induces IR divergence in (A19).

To understand the reason for this let us recall the order of IR divergence $\mathbb{I}_{19}\mathbb{I}_{248}\mathbb{R}_{567} M^{\mathrm{R}}_{\mathrm{X253}}$. The IR divergence associated with $\mathcal{S}_1$ (that corresponds to $\mathbb{I}_{19}$) is a necessary condition of the IR divergence associated with $\mathcal{S}_3$ (that corresponds to $\mathbb{I}_{248}$), since the reduced subdiagram $\{1\ 9;\ a\}$ is *included* in the reduced subdiagram $\{1\ 2\ 4\ 5\ 6\ 7\ 8\ 9;\ a\ b\ d\ e\}$. Similarly, the simultaneous IR divergence of $\mathbb{I}_{19}$ and $\mathbb{I}_{248}$ is the necessary condition of the self-mass term of dm^{R}_{4a}. This suggests that the diagram X253 should have the IR divergence of the form

$$L^{\mathrm{R}}_2(1,9)\, L_{2^*}(2,4,8)\, dm_{4a}(5,6,7)\, M_2(3), \tag{A20}$$

where we indicate the lepton lines consisting of each terms in the parenthesis. The mass-renormalization term $dm_{4a}(5,6,7)$ can be exactly removed by K-operation and R-subtraction as described before.

The I-operation encoded in GENCODEN creates an IR subtraction term of the form

$$L^{\rm R} = L - L^{\rm UV} - \text{UV divergences of subdiagrams} \tag{A21}$$

for the vertex renormalization constant L. (See (32) for the precise definition.) By the construction of K-operation, $L^{\rm UV}$ is identified as the *maximally-contracted* term. (See Ref. [22].) When the I-subtraction is accompanied by the R-subtraction from inner part of the diagram, it yields the term of the form L^* where $*$ stands for the insertion of a two-point vertex in one of the lepton lines of L. GENCODEN ignores this difference in the IR-subtraction step and applies the same rule to L^* and L, constructing the IR subtraction term of the form

$$\tilde{L}^{*\rm R} = L^* - L^*\big|_{\text{max. contr.}} - \text{UV divergences of subdiagrams.} \tag{A22}$$

Note that $\tilde{L}^{*\rm R}$ is distinguished from $L^{*\rm R} = L^* - (\text{UV divergences of subdiagrams})$, where L^* does not suffer from an overall UV divergence as is easily seen by UV power counting. We may use $\tilde{L}^{*\rm R}$ instead of $L^{*\rm R}$ in order to subtract IR divergence. The difference simply results in the additional and finite residual renormalization terms proportional to $\Delta L^*\ \Delta dm$ that have been correctly incorporated in our calculation.

For some specific diagrams in which the structure L^* appears inside of another IR-divergent structure L^R, the finite contribution of $L^*\big|_{\text{max. contr.}}$ induces spurious IR divergence. To see this, let us go back to our case of X253 and express the *contraction structure* of $L_{4b2(2^*)}$ in Eq. (A18) symbolically as $L_{4b2(2^*)} \equiv F_0 + F_1 + F_2$, where F_i is the term with i contractions. F_2 corresponds to $L_{4b2(2^*)}\big|_{\text{max. contr.}}$ and $F_0 + F_1$ corresponds to $\tilde{L}_{4b2(2^*)}$. The IR-divergence structure of $L_{4b2(2^*)}$ can be isolated by the $\mathbb{I}_{19}$ operation as

$$\mathbb{I}_{19} L^{\rm R}_{4b2(2^*)} = L^{\rm R}_2 L_{2^*}. \tag{A23}$$

After extraction of $L^{\rm R}_2$ by the $\mathbb{I}_{19}$-operation, the remaining factor has the contraction structure $F_0 + F_1$, where F_0 and F_1 correspond to $\tilde{L}^{\rm R}_{2^*}$ and ΔL_{2^*}, respectively. Substituting (A23) in (A18) one finds that the result is different from (A19) by

$$L^{\rm R}_2\ \Delta L_{2^*}\ dm^{\rm R}_{4a}\ M_2, \tag{A24}$$

which is logarithmically IR-divergent due to the presence of $L_2^{\rm R}$. Since L_{2^*} is UV-finite, there is no $L_{2^*}^{\rm UV}$ to be subtracted by the K-operation. Thus the I-operation as defined in GENCODEN yields spurious IR divergence for $M_{\rm X253}$. At present this is corrected by adding (A24) to (A19) manually. This modification had been adopted in the calculation presented in Ref. [9].

Note that the spurious divergent term in GENCODEN emerges first at 10th order. It occurs when there are nested I-operations and the inner part also involves self-mass subtraction. Since R-subtractions are applied to fourth or higher order self-energy-like subdiagrams, the total order of diagram should be at least 10. There are only two diagrams in 10th order, $X253$ and $X256$.

To summarize, the IR divergences of $M_{\rm X253}^{\rm R}$ can be separated by considering all combination of R- and I-subtractions. After separating IR-divergent and IR-finite parts of other terms of (A14) in the same fashion, we obtain:

$$\begin{aligned}
a_{\rm X253} &= \Delta M_{\rm X253} + \Delta M_{16}\ L_2^{\rm R} - \Delta M_{42}\ B_2^{\rm R} - 2\Delta M_{30}\ L_2^{\rm R} \\
&\quad - 2\Delta M_{6a}\ (L_2^{\rm R})^2 + \Delta M_{6b}\ (4\ L_2^{\rm R}\ B_2^{\rm R} - B_{4a}^{\rm R}) - \Delta M_{6c}\ L_2^{\rm R}\ B_2^{\rm R} \\
&\quad + \Delta M_{4a}\ \{-B_2^{\rm R}\ L_{4b2}^{\rm R} + L_{6b(2)}^{\rm R}\} \\
&\quad + \Delta M_{4b}\ \{-2\ L_2^{\rm R}\ (B_2^{\rm R})^2 + 4\ (L_2^{\rm R})^2\ B_2^{\rm R} + B_{4a}^{\rm R}\ (B_2^{\rm R} - L_2^{\rm R})\} \\
&\quad + M_2\ dm_{4a}^{\rm R}\ (-\tilde{L}_{4b2(2^*)}^{\rm R} + B_{4b(1^*)}^{\rm R} - B_{2^*}\ B_2^{\rm R}) \\
&\quad + M_2\ [L_{42(2)}^{\rm R} - B_{16}^{\rm R} + B_{6c}^{\rm R}\ B_2^{\rm R} + 2\ B_{6a}^{\rm R}\ L_2^{\rm R} - 4\ L_{6b(2)}^{\rm R}\ L_2^{\rm R} \\
&\qquad + 4\ L_{4b2}^{\rm R}\ L_2^{\rm R}\ B_2^{\rm R} + B_{4a}^{\rm R}\ \{B_{4b}^{\rm R} - L_{4b2}^{\rm R} - (B_2^{\rm R})^2 + L_2^{\rm R}\ B_2^{\rm R}\} \\
&\qquad - 4\ B_{4b}^{\rm R}\ L_2^{\rm R}\ B_2^{\rm R} + 2\ L_2^{\rm R}\ (B_2^{\rm R})^2 (B_2^{\rm R} - L_2^{\rm R})]\ . \qquad \text{(A25)}
\end{aligned}$$

Appendix B: Summing up Residual Renormalization Terms of Set V

1. Preliminary remarks

The total number of residual renormalization terms contributing to the Set V of the tenth-order $g-2$ exceeds 11,000. Evaluating these integrals individually and then combining them into one could become intractable unless they are organized systematically. Fortunately, it is possible to express them in terms of lower-order $g-2$ and finite parts of lower-order renormalization constants. In this Appendix we will present our result following the pattern described for lower-order cases in Appendix A of Ref. [19].

Throughout this article we are concerned only with the diagrams of q-type, namely diagrams without closed lepton loops. M_n, $n = 2, 4, \cdots$, refers to the magnetic moment projection of the sum of the set of unrenormalized vertex amplitudes transformed by means of the Ward-Takahashi identity (19), given in the form

$$M_{10} = \sum_{\alpha=001}^{389} \eta_\alpha M_\alpha, \qquad M_8 = \sum_{\alpha=01}^{47} \eta_\alpha M_\alpha,$$
$$M_6 = \sum_{\alpha=A}^{H} \eta_\alpha M_\alpha, \qquad M_4 = M_{4a} + M_{4b}, \tag{B1}$$

where $\eta_\alpha = 1$ for the time-reversal-symmetric diagrams and $\eta_\alpha = 2$ otherwise. Quantities such as L_n, B_n, and dm_n refer to the on-shell renormalization constants of vertex, wave-function, and mass renormalization types. The quantity L_{2^*} means a diagram derived from L_2 by insertion of a two-point vertex in the lepton line. L_{4^*} represents the set of diagrams obtained by insertion of a two-point vertex in the lepton lines of L_4 in all possible ways. M_{n^*}, L_{n^*}, B_{n^*}, and dm_{n^*} are defined similarly. $M_{n^{**}}$, $L_{n^{**}}$, $B_{n^{**}}$, and $dm_{n^{**}}$ are insertion of two two-point vertices in the lepton lines of M_n, L_n, B_n, and dm_n, and so on.

The UV-divergent part of quantities defined by the K-operation is identified by the superscript UV. Quantities with the superscript R are the UV-finite parts that remain after all UV-divergent parts, including UV divergences of subdiagrams, are subtracted out. Symbols with prefix Δ mean UV- and IR-finite quantities.

In order to make the process of residual renormalization transparent it is useful to treat UV-divergence subtraction, R-subtraction, and IR-divergence subtraction, separately, since K-operation and I-operation correspond to different divergence structures. Diagrams X253 and X256 require some modification of the I-operation. This is discussed in Appendix A.

2. Standard on-the-mass-shell renormalization of $A_1^{(10)}$[Set V]

The tenth-order magnetic moment $A_1^{(10)}$[Set V] has contributions from 389 WT-summed diagrams shown in Fig. 1. In the standard renormalization it can be written in terms of unrenormalized amplitudes M_{10}, M_8, M_6, *etc.*, and various renormalization constants as follows:

$$A_1^{(10)}[\text{Set V}] = \Xi_1 + \Xi_2 + \Xi_3 + \Xi_4 + \Xi_5, \tag{B2}$$

where

$$
\begin{aligned}
\Xi_1 = {} & M_{10} \\
& + M_8(-7B_2 - 8L_2) \\
& + M_6(-5B_4 - 6L_4 + 20B_2^2 + 52B_2L_2 + 33L_2^2) \\
& + M_4(-3B_6 - 4L_6 + 24B_4B_2 + 32B_4L_2 + 34B_2L_4 + 44L_2L_4 \\
& \quad - 28B_2^3 - 128B_2^2L_2 - 187B_2L_2^2 - 88L_2^3) \\
& + M_2(-B_8 - 2L_8 + 8B_6B_2 + 12B_6L_2 + 16B_2L_6 + 22L_6L_2 \\
& \quad + 4B_4^2 - 28B_4B_2^2 - 96B_4B_2L_2 + 14B_4L_4 - 77B_4L_2^2 \\
& \quad + 14B_2^4 + 112B_2^3L_2 - 56B_2^2L_4 \\
& \quad + 308B_2^2L_2^2 - 176B_2L_2L_4 + 352B_2L_2^3 \\
& \quad + 11L_4^2 - 132L_4L_2^2 + 143L_2^4), \qquad \text{(B3)}
\end{aligned}
$$

$$
\begin{aligned}
\Xi_2 = {} & M_{8^*}dm_2(-1) \\
& + M_{6^*}dm_2(7B_2 + 8L_2) \\
& + M_{4^*}dm_2(5B_4 + 6L_4 - 20B_2^2 - 52B_2L_2 - 33L_2^2) \\
& + M_{2^*}dm_2(3B_6 - 32L_2B_4 + 88L_2^3 - 44L_4L_2 + 4L_6 - 24B_2B_4 \\
& \quad + 187B_2L_2^2 - 34B_2L_4 + 128B_2^2L_2 + 28B_2^3) \\
& + M_6dm_2(5B_{2^*} + 12L_{2^*}) \\
& + M_4dm_2(3B_{4^*} + 4L_{4^*} - 24B_2B_{2^*} - 68B_2L_{2^*} - 32L_2B_{2^*} - 88L_2L_{2^*}) \\
& + M_2dm_2(B_{6^*} + 2L_{6^*} - 8B_2B_{4^*} - 16B_2L_{4^*} \\
& \quad + 28B_2^2B_{2^*} + 112B_2^2L_{2^*} + 96B_2L_2B_{2^*} \\
& \quad + 352B_2L_2L_{2^*} - 12L_2B_{4^*} - 22L_2L_{4^*} + 77L_2^2B_{2^*} \\
& \quad + 264L_2^2L_{2^*} - 8B_{2^*}B_4 - 14B_{2^*}L_4 - 28L_{2^*}B_4 - 44L_{2^*}L_4), \qquad \text{(B4)}
\end{aligned}
$$

$$
\begin{aligned}
\Xi_3 = {} & M_{6^*} dm_4(-1) \\
& + M_{6^*} dm_2 dm_{2^*} \\
& + M_{4^*} dm_4(7B_2 + 8L_2) \\
& + M_{4^*} dm_2 dm_{2^*}(-7B_2 - 8L_2) \\
& + M_{2^*} dm_4(5B_4 + 6L_4 - 20B_2^2 - 52B_2L_2 - 33L_2^2) \\
& + M_{2^*} dm_2 dm_{2^*}(-5B_4 - 6L_4 + 20B_2^2 + 52B_2L_2 + 33L_2^2) \\
& + M_4 dm_4(3B_{2^*} + 8L_{2^*}) \\
& + M_4 dm_2 dm_{2^*}(-3B_{2^*} - 8L_{2^*}) \\
& + M_2 dm_4(B_{4^*} + 2L_{4^*} - 8B_2B_{2^*} - 32B_2L_{2^*} - 12L_2B_{2^*} - 44L_2L_{2^*}) \\
& + M_2 dm_2 dm_{2^*}(-B_{4^*} - 2L_{4^*} + 8B_2B_{2^*} + 32B_2L_{2^*} + 12L_2B_{2^*} + 44L_2L_{2^*}) \\
& + M_{6^{**}} dm_2^2 \\
& + M_{4^{**}} dm_2^2(-7B_2 - 8L_2) \\
& + M_{2^{**}} dm_2^2(-5B_4 - 6L_4 + 20B_2^2 + 52B_2L_2 + 33L_2^2) \\
& + M_{4^*} dm_2^2(-5B_{2^*} - 12L_{2^*}) \\
& + M_{2^*} dm_2^2(-3B_{4^*} - 4L_{4^*} + 24B_2B_{2^*} + 68B_2L_{2^*} + 32L_2B_{2^*} + 88L_2L_{2^*}) \\
& + M_4 dm_2^2(-3B_{2^{**}} - 4L_{2^{**}}) \\
& + M_2 dm_2^2(-B_{4^{**}} - 2L_{4^{**}} + 8B_2B_{2^{**}} + 44L_{2^*}^2 \\
& \quad + 16B_2L_{2^{**}} + 12L_2B_{2^{**}} + 22L_2L_{2^{**}} + 4B_{2^*}^2 + 28B_{2^*}L_{2^*}),
\end{aligned}
\tag{B5}
$$

$$
\begin{aligned}
\Xi_4 = {} & M_{4^*} dm_6(-1) \\
& + M_{4^*} dm_2 dm_{4^*} \\
& + M_{4^*} dm_4 dm_{2^*} \\
& + M_{4^*} dm_2 dm_{2^*}^2(-1) \\
& + M_{4^*} dm_2^2 dm_{2^{**}}(-1) \\
& + M_{2^*} dm_6(7B_2 + 8L_2) \\
& + M_{2^*} dm_2 dm_{4^*}(-7B_2 - 8L_2) \\
& + M_{2^*} dm_4 dm_{2^*}(-7B_2 - 8L_2) \\
& + M_{2^*} dm_2 dm_{2^*}^2(7B_2 + 8L_2) \\
& + M_{2^*} dm_2^2 dm_{2^{**}}(7B_2 + 8L_2) \\
& + M_2 dm_6(B_{2^*} + 4L_{2^*}) \\
& + M_2 dm_2 dm_{4^*}(-B_{2^*} - 4L_{2^*}) \\
& + M_2 dm_4 dm_{2^*}(-B_{2^*} - 4L_{2^*}) \\
& + M_2 dm_2 dm_{2^*}^2(B_{2^*} + 4L_{2^*}) \\
& + M_2 dm_2^2 dm_{2^{**}}(B_{2^*} + 4L_{2^*}) \\
& + M_{4^{**}} dm_2 dm_4(2) \\
& + M_{4^{**}} dm_2^2 dm_{2^*}(-2) \\
& + M_{2^{**}} dm_2 dm_4(-14B_2 - 16L_2) \\
& + M_{2^{**}} dm_2^2 dm_{2^*}(14B_2 + 16L_2) \\
& + M_{2^*} dm_2 dm_4(-8B_{2^*} - 20L_{2^*}) \\
& + M_{2^*} dm_2^2 dm_{2^*}(8B_{2^*} + 20L_{2^*}) \\
& + M_2 dm_2 dm_4(-2B_{2^{**}} - 4L_{2^{**}}) \\
& + M_2 dm_2^2 dm_{2^*}(2B_{2^{**}} + 4L_{2^{**}}) \\
& + M_{4^{***}} dm_2^3(-1) \\
& + M_{2^{***}} dm_2^3(7B_2 + 8L_2) \\
& + M_{2^{**}} dm_2^3(5B_{2^*} + 12L_{2^*}) \\
& + M_{2^*} dm_2^3(3B_{2^{**}} + 4L_{2^{**}}) \\
& + M_2 dm_2^3(B_{2^{***}} + 2L_{2^{***}}),
\end{aligned}
\tag{B6}
$$

$$
\begin{aligned}
\Xi_5 = {} & M_{2^*} dm_8(-1) \\
& + M_{2^*} dm_2 dm_{6^*} \\
& + M_{2^*} dm_4 dm_{4^*} \\
& + M_{2^*} dm_2 dm_{2^*} dm_{4^*}(-2) \\
& + M_{2^*} dm_2^2 dm_{4^{**}}(-1) \\
& + M_{2^*} dm_6 dm_{2^*} \\
& + M_{2^*} dm_4 dm_{2^*}^2(-1) \\
& + M_{2^*} dm_2 dm_{2^*}^3 \\
& + M_{2^*} dm_2^2 dm_{2^*} dm_{2^{**}}(3) \\
& + M_{2^*} dm_2 dm_{2^{**}} dm_4(-2) \\
& + M_{2^*} dm_2^3 dm_{2^{***}} \\
& + M_{2^{**}} dm_2 dm_6(2) \\
& + M_{2^{**}} dm_2^2 dm_{4^*}(-2) \\
& + M_{2^{**}} dm_4^2 \\
& + M_{2^{**}} dm_2 dm_{2^*} dm_4(-4) \\
& + M_{2^{**}} dm_2^2 dm_{2^*}^2(3) \\
& + M_{2^{**}} dm_2^3 dm_{2^{**}}(2) \\
& + M_{2^{***}} dm_2^2 dm_4(-3) \\
& + M_{2^{***}} dm_2^3 dm_{2^*}(3) \\
& + M_{2^{****}} dm_2^4. \qquad \text{(B7)}
\end{aligned}
$$

Terms containing self-mass subdiagrams are numerous but can be readily identified since they always accompany some B_n. For instance, $-M_{8^*} dm_2$ accompanies $-7M_8 B_2$.

3. Treatment of UV divergences by the K-operation

Terms listed in Eqs. (B3), (B4), (B5), (B6), and (B7) are all UV-divergent. Application of K-operations to each of these integrals extracts UV-divergent parts. The resulting UV-finite part will be denoted as M_n^{R}, etc. See Eqs. (27), (30), and (32). K-operations applied

to M_{10}, the first term of (B3), give rise to $M_{10}^{\rm R}$:

$$\begin{aligned} M_{10}^{R} &= M_{10} \\ &+ M_8(-7B_2^{UV} - 8L_2^{UV}) \\ &+ M_6(-5B_4^{UV} - 6L_4^{UV} + 20(B_2^{UV})^2 + 52B_2^{UV}L_2^{UV} + 33(L_2^{UV})^2) \\ &+ M_4(-3B_6^{UV} - 4L_6^{UV} + 24B_4^{UV}B_2^{UV} + 32B_4^{UV}L_2^{UV} + 34B_2^{UV}L_4^{UV} + 44L_2^{UV}L_4^{UV} \\ &\quad -28(B_2^{UV})^3 - 128(B_2^{UV})^2L_2^{UV} - 187B_2^{UV}(L_2^{UV})^2 - 88(L_2^{UV})^3) + \ldots, \end{aligned} \tag{B8}$$

where the remaining terms are not shown explicitly, but can be readily found since the coefficients of all UV-divergent terms of (B8) are the same as those of standard renormalization formula (B2).

Solving (B8) for M_{10} and substituting these terms in (B2), one can express $A_1^{(10)}$[Set V] in terms of $M_{10}^{\rm R}$, M_8, M_6, etc. Next, replace M_8 by $M_8^{\rm R}$, etc., using Eq. (A24) of Ref. [19]. The result still contains M_6, which can be replaced by $M_6^{\rm R}$ using Eq. (A14) of Ref. [19], and so on. We also have to extract UV-finite parts of renormalization constants L_n, B_n, dm_n, etc. In this way we arrive at the expression of $A_1^{(10)}$[Set V] as the sum of UV-finite quantities only:

$$\begin{aligned} A_1^{(10)}[\text{Set V}] &= M_{10}^{\rm R} \\ &+ M_8^{\rm R}(-7B_2^{\rm R} - 8L_2^{\rm R}) \\ &+ M_6^{\rm R}(-5B_4^{\rm R} - 6L_4^{\rm R} + 20(B_2^{\rm R})^2 + 52B_2^{\rm R}L_2^{\rm R} + 33(L_2^{\rm R})^2) \\ &+ M_4^{\rm R}(-3B_6^{\rm R} - 4L_6^{\rm R} + 24B_2^{\rm R}B_4^{\rm R} + 32L_2^{\rm R}B_4^{\rm R} + 34B_2^{\rm R}L_4^{\rm R} + 44L_2^{\rm R}L_4^{\rm R} \\ &\quad - 28(B_2^{\rm R})^3 - 128(B_2^{\rm R})^2L_2^{\rm R} - 187B_2^{\rm R}(L_2^{\rm R})^2 - 88(L_2^{\rm R})^3) \\ &+ M_2(-B_8^{\rm R} - 2L_8^{\rm R} + 8B_6^{\rm R}B_2^{\rm R} + 12L_2^{\rm R}B_6^{\rm R} + 16B_2^{\rm R}L_6^{\rm R} + 22L_2^{\rm R}L_6^{\rm R} \\ &\quad + 4(B_4^{\rm R})^2 - 28(B_2^{\rm R})^2B_4^{\rm R} - 96B_2^{\rm R}L_2^{\rm R}B_4^{\rm R} + 14L_4^{\rm R}B_4^{\rm R} - 77(L_2^{\rm R})^2B_4^{\rm R} \\ &\quad + 14(B_2^{\rm R})^4 + 112(B_2^{\rm R})^3L_2^{\rm R} - 56(B_2^{\rm R})^2L_4^{\rm R} \\ &\quad + 308(B_2^{\rm R})^2(L_2^{\rm R})^2 - 176B_2^{\rm R}L_2^{\rm R}L_4^{\rm R} + 352(L_2^{\rm R})^3B_2^{\rm R} \\ &\quad + 11(L_4^{\rm R})^2 - 132(L_2^{\rm R})^2L_4^{\rm R} + 143(L_2^{\rm R})^4) \\ &+ M_4^{\rm R}dm_4^{\rm R}(3B_{2^*} + 8L_{2^*}) \\ &+ M_2dm_4^{\rm R}(B_{4^*}^{\rm R} + 2L_{4^*}^{\rm R}) \\ &+ M_2dm_4^{\rm R}(-12B_{2^*}L_2^{\rm R} - 8B_2^{\rm R}B_{2^*} - 44L_{2^*}L_2^{\rm R} - 32B_2^{\rm R}L_{2^*}) \end{aligned}$$

$$
\begin{aligned}
&+ M_2 dm_6^{\rm R}(B_{2^*} + 4L_{2^*}) \\
&+ M_2 dm_4^{\rm R} dm_{2^*}^{\rm R}(-B_{2^*} - 4L_{2^*}) \\
&+ M_{6^*}^{\rm R}(-dm_4^{\rm R}) \\
&+ M_{4^*}^{\rm R} dm_4^{\rm R}(7B_2^{\rm R} + 8L_2^{\rm R}) \\
&+ M_{2^*} dm_4^{\rm R}(-52L_2^{\rm R}B_2^{\rm R} - 33(L_2^{\rm R})^2 - 20(B_2^{\rm R})^2 + 5B_4^{\rm R} + 6L_4^{\rm R}) \\
&+ M_{4^*}^{\rm R}(-dm_6^{\rm R} + dm_4^{\rm R} dm_{2^*}^{\rm R}) \\
&+ M_{2^*} dm_6^{\rm R}(7B_2^{\rm R} + 8L_2^{\rm R}) \\
&+ M_{2^*} dm_4^{\rm R} dm_{2^*}^{\rm R}(-7B_2^{\rm R} - 8L_2^{\rm R}) \\
&+ M_{2^*}(-dm_8^{\rm R}) \\
&+ M_{2^*}(dm_4^{\rm R} dm_{4^*}^{\rm R} + dm_{2^*}^{\rm R} dm_6^{\rm R} - (dm_{2^*}^{\rm R})^2 dm_4^{\rm R}) \\
&+ M_{2^{**}}(dm_4^{\rm R})^2. \qquad \text{(B9)}
\end{aligned}
$$

Note that Eq. (B9) has exactly the same structure as (B2). Apparent dramatic simplification of (B9) is a consequence of the fact that $dm_2^{\rm R}$ vanishes according to the definition of K-operation. This is what one would expect since all UV-divergent quantities in (B2) must cancel out after K-operation is carried out, leaving only UV-finite pieces with their original numerical coefficients unchanged.

4. *R*-subtraction

Eight of the last nine lines of Eq. (B9) containing M_{2^*}, $M_{4^*}^{\rm R}$, and $M_{6^*}^{\rm R}$, are linearly IR-divergent. The last line proportional to $M_{2^{**}}$ is even more singular, being quadratically IR-divergent. They are all characterized by the fact that they contain one of the factors $dm_4^{\rm R}$, $dm_6^{\rm R}$, or $dm_8^{\rm R}$, which are UV-finite remnants of dm_4, dm_6, or dm_8, after their UV-divergent parts are removed by the K-operation. Since $A_1^{(10)}$[Set V] as a whole is IR-finite, these IR-divergent terms must cancel linear or quadratic IR divergences hidden in $M_8^{\rm R}$ and $M_{10}^{\rm R}$. The R-subtraction is a procedure to combine and cancel out corresponding IR divergences of $M_8^{\rm R}$ or $M_{10}^{\rm R}$ with those of the last nine lines of (B9), which amounts to redefining $M_8^{\rm R}$ and $M_{10}^{\rm R}$. The last nine lines of (B9) must be dropped after $M_8^{\rm R}$ and $M_{10}^{\rm R}$ are redefined. This procedure is incorporated in GENCODEN as its integral part.

5. Separation of IR divergences by *I*-operation

After linear IR divergences are removed by the *R*-subtraction we still have to deal with logarithmic IR divergences. This can be readily handled by the *I*-operation. However, the *I*-operation incorporated in the program GENCODE*N* requires a slight modification for the diagrams X253 and X256, which is described in Appendix A.

The result of the *I*-operation can be factorized analytically into the product of UV-finite parts of lower-order renormalization constant and anomalous magnetic moment as is shown in Eq. (33). The individual UV-finite terms of (B9) are expressed as sums of IR-divergent parts and IR-finite parts (which are indicated by the prefix Δ). The sums of the finite magnetic moment amplitudes of the nth-order are given in terms of UV-finite quantities as follows:

$$\begin{aligned}
\Delta M_{10} &= M_{10}^{\rm R} - M_8^{\rm R} L_2^{\rm R} - M_6^{\rm R}(L_4^{\rm R} - (L_2^{\rm R})^2) \\
&\quad - M_4^{\rm R}(L_6^{\rm R} - 2L_2^{\rm R}L_4^{\rm R} + (L_2^{\rm R})^3 - 2\tilde{L}_{2^*}^{\rm R} dm_4^{\rm R}) \\
&\quad - M_2(L_8^{\rm R} - 2L_2^{\rm R}L_6^{\rm R} - (L_4^{\rm R})^2 + 3(L_2^{\rm R})^2 L_4^{\rm R} - (L_2^{\rm R})^4 \\
&\qquad - 2\tilde{L}_{2^*}^{\rm R} dm_6^{\rm R} + 2\tilde{L}_{2^*}^{\rm R} dm_{2^*}^{\rm R} dm_4^{\rm R} + 2\tilde{L}_{2^*}^{\rm R} L_2^{\rm R} dm_4^{\rm R} + 2L_2^{\rm R} L_{2*} dm_4^{\rm R} - \tilde{L}_{4^*}^{\rm R} dm_4^{\rm R}) \\
&\quad - M_{6^*}^{\rm R} dm_4^{\rm R} \\
&\quad - M_{4^*}^{\rm R}(dm_6^{\rm R} - dm_4^{\rm R} L_2^{\rm R} - dm_{2^*}^{\rm R} dm_4^{\rm R}) \\
&\quad - M_{2^*}(dm_8^{\rm R} - dm_{4^*}^{\rm R} dm_4^{\rm R} + (dm_{2^*}^{\rm R})^2 dm_4^{\rm R} - dm_{2^*}^{\rm R} dm_6^{\rm R} \\
&\qquad - dm_6^{\rm R} L_2^{\rm R} + dm_{2^*}^{\rm R} dm_4^{\rm R} L_2^{\rm R} - dm_4^{\rm R} L_4^{\rm R} + dm_4^{\rm R}(L_2^{\rm R})^2) \\
&\quad + M_{2^{**}}(dm_4^{\rm R})^2, \qquad \text{(B10)} \\
\Delta M_8 &= M_8^{\rm R} - M_6^{\rm R} L_2^{\rm R} - M_4^{\rm R}(L_4^{\rm R} - (L_2^{\rm R})^2) \\
&\quad - M_2^{\rm R}(L_6^{\rm R} - 2L_4^{\rm R} L_2^{\rm R} + (L_2^{\rm R})^3 - 2\tilde{L}_{2^*}^{\rm R} dm_4^{\rm R}) \\
&\quad - M_{2^*}(dm_6^{\rm R} - dm_{2^*}^{\rm R} dm_4^{\rm R} - dm_4^{\rm R} L_2^{\rm R}) \\
&\quad - M_{4^*}^{\rm R} dm_4^{\rm R}, \qquad \text{(B11)} \\
\Delta M_6 &= M_6^{\rm R} - M_4^{\rm R} L_2^{\rm R} - M_2(L_4^{\rm R} - (L_2^{\rm R})^2) - M_{2^*} dm_4^{\rm R}, \qquad \text{(B12)} \\
\Delta M_4 &= M_4^{\rm R} - M_2 L_2^{\rm R}. \qquad \text{(B13)}
\end{aligned}$$

The finite integrals derived from the renormalization constants are:

$$
\begin{aligned}
\Delta LB_8 &= L_8^{\rm R} + B_8^{\rm R} - \{L_6^{\rm R} - 2L_4^{\rm R}L_2^{\rm R} + (L_2^{\rm R})^3\}(L_2^{\rm R} + B_2^{\rm R}) \\
&\quad - \{L_4^{\rm R} - (L_2^{\rm R})^2\}(L_4^{\rm R} + B_4^{\rm R}) - L_2^{\rm R}(L_6^{\rm R} + B_6^{\rm R}) \\
&\quad - \{dm_6^{\rm R} - (L_2^{\rm R} + dm_{2^*}^{\rm R})dm_4^{\rm R}\}(2L_{2^*} + B_{2^*}) \\
&\quad + 2\tilde{L}_{2^*}^{\rm R} dm_4^{\rm R}(L_2^{\rm R} + B_2^{\rm R}) - dm_4^{\rm R}(L_{4^*}^{\rm R} + B_{4^*}^{\rm R}), \\
\Delta LB_6 &= L_6^{\rm R} + B_6^{\rm R} - \{L_4^{\rm R} - (L_2^{\rm R})^2\}(L_2^{\rm R} + B_2^{\rm R}) - L_2^{\rm R}(L_4^{\rm R} + B_4^{\rm R}) \\
&\quad - dm_4^{\rm R}(2L_{2^*} + B_{2^*}), \\
\Delta LB_4 &= L_4^{\rm R} + B_4^{\rm R} - L_2^{\rm R}(L_2^{\rm R} + B_2^{\rm R}), \\
\Delta LB_2 &= L_2^{\rm R} + B_2^{\rm R}, \\
\Delta dm_6 &= dm_6^{\rm R} - L_2^{\rm R} dm_4^{\rm R}, \\
\Delta dm_4 &= dm_4^{\rm R} \ .
\end{aligned}
\tag{B14}
$$

(See Appendix A for the quantities $\tilde{L}_{2^*}^{\rm R}$ and $\tilde{L}_{4^*}^{\rm R}$.)

Substituting Eqs. (B10)–(B14) in (B9), we can transform $A_1^{(10)}$[Set V] into the sum of terms which are completely free from UV- and IR-divergences:

$$
\begin{aligned}
A_1^{(10)}[\text{Set V}] \ &= \ \Delta M_{10} \\
&+ \ \Delta M_8(-7\Delta LB_2) \\
&+ \ \Delta M_6(20(\Delta LB_2)^2 - 5\Delta LB_4) \\
&+ \ \Delta M_4(24\Delta LB_2\Delta LB_4 - 28(\Delta LB_2)^3 - 3\Delta LB_6) \\
&+ \ M_2(8\Delta LB_2\Delta LB_6 - 28(\Delta LB_2)^2\Delta LB_4) \\
&+ \ M_2(14(\Delta LB_2)^4 + 4(\Delta LB_4)^2 - \Delta LB_8) \\
&+ \ 2\Delta M_4\Delta L_{2^*}\Delta dm_4 \\
&+ \ 2M_2\Delta L_{2^*}\Delta dm_6 \\
&+ \ M_2\Delta L_{4^*}\Delta dm_4 \\
&- \ 16M_2\Delta L_{2^*}\Delta LB_2\Delta dm_4 \\
&- \ 2M_2\Delta L_{2^*}\Delta dm_{2^*}\Delta dm_4,
\end{aligned}
\tag{B15}
$$

where $\Delta L_{4^*} = L_{4^*}^{\rm R} - \tilde{L}_{4^*}^{\rm R}$, and $\Delta L_{2^*} = L_{2^*} - \tilde{L}_{2^*}^{\rm R}$. The values of ΔL_{2^*}, ΔL_{4^*}, Δdm_6, and Δdm_{2^*} are listed in Table II.

Note that the last five terms of (B15), even though they contain factors such as Δdm_4 and Δdm_6, are not removed by the R-subtraction. This is because the factors ΔL_{2^*} and ΔL_{4^*} are not IR-divergent so that the R-subtraction rule does not apply to them. As a matter of fact they are indefinite, although finite, since they depend on how the IR-divergent parts I_{2^*} and I_{4^*} are defined. However, this does not cause difficulty since these terms must be canceled by the corresponding terms hidden in ΔM_{10} and ΔM_8. Actually this is an artifact caused by our definition of R-subtraction and I-operation adopted in the program GENCODEN which subtracts only the IR-divergent parts I_{2^*} and I_{4^*} instead of full L_{2^*} and L_{4^*}. The value of A_1^{10}[Set V] is unambiguous as far as the I-operation is carried out consistently throughout the calculation.

---

[1] D. Hanneke, S. Fogwell, and G. Gabrielse, Phys. Rev. Lett. **100**, 120801 (2008).
[2] D. Hanneke, S. Fogwell Hoogerheide, and G. Gabrielse, Phys. Rev. A **83**, 052122 (2011).
[3] S. F. Hoogerheide, Ph.D. thesis, Harvard University (2013), http://nrs.harvard.edu/urn-3:HUL.Instrepos:10985007.
[4] P. J. Mohr, B. N. Taylor, and D. B. Newell, Rev. Mod. Phys. **84**, 1527 (2012).
[5] J. S. Schwinger, Phys. Rev. **73**, 416 (1948).
[6] A. Petermann, Helv. Phys. Acta **30**, 407 (1957).
[7] C. M. Sommerfield, Ann. Phys. (N.Y.) **5**, 26 (1958).
[8] S. Laporta and E. Remiddi, Phys. Lett. **B379**, 283 (1996).
[9] T. Aoyama, M. Hayakawa, T. Kinoshita, and M. Nio, Phys. Rev. Lett. **109**, 111807 (2012).
[10] G. P. Lepage, J. Comput. Phys. **27**, 192 (1978).
[11] T. Kinoshita and M. Nio, Phys. Rev. D **73**, 053007 (2006).
[12] T. Aoyama, M. Hayakawa, T. Kinoshita, M. Nio, and N. Watanabe, Phys. Rev. D **78**, 053005 (2008).
[13] T. Aoyama, M. Hayakawa, T. Kinoshita, and M. Nio, Phys. Rev. D **78**, 113006 (2008).
[14] T. Aoyama, K. Asano, M. Hayakawa, T. Kinoshita, M. Nio, and N. Watanabe, Phys. Rev. D **81**, 053009 (2010).
[15] T. Aoyama, M. Hayakawa, T. Kinoshita, and M. Nio, Phys. Rev. D **82**, 113004 (2010).
[16] T. Aoyama, M. Hayakawa, T. Kinoshita, and M. Nio, Phys. Rev. D **83**, 053003 (2011).
[17] T. Aoyama, M. Hayakawa, T. Kinoshita, and M. Nio, Phys. Rev. D **83**, 053002 (2011).
[18] T. Aoyama, M. Hayakawa, T. Kinoshita, and M. Nio, Phys. Rev. D **84**, 053003 (2011).
[19] T. Aoyama, M. Hayakawa, T. Kinoshita, and M. Nio, Phys. Rev. D **85**, 033007 (2012).
[20] T. Aoyama, M. Hayakawa, T. Kinoshita, and M. Nio, Phys. Rev. D **85**, 093013 (2012).
[21] P. Baikov, A. Maier, and P. Marquard, Nucl. Phys. **B877**, 647 (2013).
[22] T. Aoyama, M. Hayakawa, T. Kinoshita, and M. Nio, Nucl. Phys. **B740**, 138 (2006).
[23] T. Aoyama, M. Hayakawa, T. Kinoshita, and M. Nio, Nucl. Phys. **B796**, 184 (2008).
[24] H. H. Elend, Phys. Lett. **20**, 682 (1966).
[25] M. A. Samuel and G.-w. Li, Phys. Rev. D **44**, 3935 (1991), erratum-ibid. **48**, 1879 (1993).
[26] G. Li, R. Mendel, and M. A. Samuel, Phys. Rev. D **47**, 1723 (1993).

[27] S. Laporta and E. Remiddi, Phys. Lett. **B301**, 440 (1993).
[28] S. Laporta, Nuovo Cim. **A106**, 675 (1993).
[29] M. Passera, Phys. Rev. D **75**, 013002 (2007).
[30] A. Kurz, T. Liu, P. Marquard, and M. Steinhauser, Nucl. Phys. **B879**, 1 (2014).
[31] A. Kataev, Phys. Rev. D **86**, 013010 (2012).
[32] G. Mishima, arXiv:1311.7109 [hep-ph].
[33] K. Melnikov, A. Vainshtein, and M. Voloshin, Phys. Rev. D **90**, 017301 (2014).
[34] M. Fael and M. Passera, Phys. Rev. D **90**, 056004 (2014).
[35] M. I. Eides, Phys. Rev. D **90**, 057301 (2014).
[36] M. A. Braun, Zh. Eksp. Teor. Fiz. **54**, 1220 (1968), [Sov. Phys. JETP **27**, 652 (1968)].
[37] R. Barbieri, P. Christillin, and E. Remiddi, Phys. Rev. A **8**, 2266 (1973).
[38] M. Hayakawa, arXiv:1403.0416 [hep-ph].
[39] D. Nomura and T. Teubner, Nucl. Phys. **B867**, 236 (2013).
[40] J. Prades, E. de Rafael, and A. Vainshtein, in *Lepton Dipole Moments*, edited by B. L. Roberts and W. J. Marciano (World Scientific, Singapore, 2009), pp. 303–319.
[41] K. Fujikawa, B. Lee, and A. Sanda, Phys. Rev. D **6**, 2923 (1972).
[42] A. Czarnecki, B. Krause, and W. J. Marciano, Phys. Rev. Lett. **76**, 3267 (1996).
[43] M. Knecht, S. Peris, M. Perrottet, and E. de Rafael, J. High Energy Phys. **11**, 003 (2002).
[44] A. Czarnecki, W. J. Marciano, and A. Vainshtein, Phys. Rev. D **67**, 073006 (2003), erratum-ibid. **73**, 119901(E) (2006).
[45] R. Bouchendira, P. Cladé, S. Guellati-Khélifa, F. Nez, and F. Biraben, Phys. Rev. Lett. **106**, 080801 (2011).
[46] P. Cvitanović and T. Kinoshita, Phys. Rev. D **10**, 3991 (1974).
[47] J. Vermaseren, math-ph/0010025.
[48] T. Kinoshita, in *Quantum electrodynamics*, edited by T. Kinoshita (World Scientific, Singapore, 1990), pp. 218–321.
[49] W. Zimmermann, Commun. Math. Phys. **15**, 208 (1969).
[50] T. Aoyama, M. Hayakawa, T. Kinoshita, and M. Nio, Phys. Rev. D **77**, 053012 (2008).
[51] Y. H. Hida, Z. S. L. Li, and D. H. Bailey, High-Precision Software Directory: `http://crd-legacy.lbl.gov/~dhbailey/mpdist/`.
[52] P. J. Mohr, B. N. Taylor, and D. B. Newell, Rev. Mod. Phys. **80**, 633 (2008).